Explicating Sediment Sources of the Catchment Upstream of the Miyun Reservoir in Beijing, China

Haiyan Fang (fanghy@igsnrr.ac.cn)
University of the Chinese Academy of Sciences https://orcid.org/0000-0002-2768-521X

Research Article

Keywords: RUSLE, SEDD, soil erosion, sediment delivery, Beijing hilly region

Posted Date: June 15th, 2021

DOI: https://doi.org/10.21203/rs.3.rs-597902/v1

Explicating sediment sources of the catchment upstream of the Miyun Reservoir in Beijing, China

Haiyan Fang[1, 2]

[1]Key Laboratory of Water Cycle and Related Land Surface Processes, Institute of Geographic Sciences and Natural Resources Research, Chinese Academy of Sciences, Beijing 100101, China

[2]College of Resources and Environment, University of Chinese Academy of Sciences, Beijing 100049, China

Abstract

As the only water drinking resource in Beijing, the Miyun Reservoir is still suffered over ten thousand tons of sediment input from its upper catchment. Explicating sediment sources of the catchment upstream of the reservoir is urgently required to further implement soil conservation measures. In this paper, the Revised Universal Soil Loss Equation (RUSLE) and Sediment Delivery (SEDD) models were combined to explicate the major sediment source of the catchment through exploring the spatial distributions of soil erosion and sediment delivery as well as their relations with land use and topography, and sediment source areas were then identified. The catchment average soil erosion intensity (SEI) of 4.08 t ha^{-1} yr^{-1} was two times the soil loss tolerance (T=2.00 t ha^{-1} yr^{-1}) of the study region. The values of cell sediment delivery ratio (SDR) showed a network distribution pattern, ranging from zero to unit, with an average of 1.65%. Cell specific sediment yield (SSY) presented a similar spatial

pattern to SDR, ranging from 0 to 902 t ha^{-1} yr^{-1}, with an average of 0.04 t ha^{-1} yr^{-1}. Bare land suffered the highest SEI of 39.01 t ha^{-1} yr^{-1}, followed by shrub land and orchard field. Nearly 70% of the sediment came from grass land. Farmland was the second sediment contributor. Grass land and farmland are the two major sediment source areas. Soil conservation practices should be further implemented on these lands, especially on the 3-5° slopes with elevations less than 500 m a.s.l.

Keywords RUSLE• SEDD• soil erosion• sediment delivery• Beijing hilly region

Introduction

Water erosion can induce both on-site and off-site environmental problems (Wilkinson et al. 2009; Modes et al. 2020). Water erosion destroys on-site soil structure, lowers soil nutrient, and degrades land. The eroded sediment can induce off-site reservoir or river sedimentation and fresh water pollution (Walling et al. 1999; Rickson 2014; Vercruysse et al. 2017; Zhao et al. 2020). Exploration of the spatial distributions of soil erosion and sediment delivery should be done before soil conservation measures are further implemented in a targeted region.

In northern China, water issue such as water shortage and water pollution has been paid attention to in recent years because it has resulted in serious problem of water supply (Zhou and Wu 2008; Tang et al. 2011; Liu and Yu 2018). For example, due to severe water pollution and heavy sediment load, the Guanting Reservoir has been excluded as a source of drinking water for Beijing, the capital of China. Currently, Miyun Reservoir has become the only source of drinking water for the

people in Beijing. Thus, water protection of the Miyun Reservoir has received great attention by local government, and soil conservation measures have widely been implemented since the 1980s in the catchment above the reservoir (Li and Li 2008). However, in recent years, mean annual sediment input from the catchment upstream to the reservoir still reaches ten thousand tons. Therefore, it is urgently required to explicate the sediment source.

In recent years, some studies which are related to sediment have been made in the catchment above the Miyun Reservoir. For example, using the Revised Universal Loss Equation (RUSLE), Feng et al. (2019) studied the impact of land use change on soil erosion in the catchment upstream of the Miyun Reservoir, but it didn't consider sediment delivery in the catchment. Zhou and Wu (2008) explored the variations of sediment deliver ratio (SDR) using the RUSLE and sediment yield (SY). Tang et al. (2011) obtained the variations of runoff, sediment concentration, and total nitrogen and total phosphorous at Xiahui and Zhangjiafen hydrological stations, based on a non-point source pollution model. Regrettably, only catchment lumped sediment delivery was considered, without considering its spatial distribution characteristics. This impedes the identification of sediment source and future land use management in the catchment.

Soil erosion modeling is an efficient and fast way to estimate soil erosion and sediment delivery in a catchment (Fang and Sun 2017; Zerihun et al. 2018). In recent decades, many models have been developed (Pandey et al. 2016). However, due to limited data availability and simplicity, the RUSLE model is the most widely used one

67 all over the world to assess spatially distributed pattern of water erosion, particularly
68 in a large catchment (Batista et al. 2017).

69 However, the RUSLE model does not consider sediment deposition, providing
70 no information of sediment delivery within a catchment (Ranzi et al. 2012; Pandey et
71 al. 2016). In fact, only part of the eroded sediment can be move out of a catchment.
72 The Sediment Delivery Distributed (SEDD) model was introduced to simulate
73 catchment sediment delivery ratio (SDR) (Di Stefano et al. 2007). The theoretical
74 approach followed by SEDD model requires a limited input data to estimate sediment
75 delivery (Fu et al. 2006; Guo et al. 2019). The combination of RUSLE and SEDD
76 models can thus provide a good approach to explicate the spatially distributed soil
77 erosion and sediment delivery, especially in regions with limited data availability.

78 In the current study, the RUSLE and SEDD models were applied to explicate the
79 sediment source through identifying the spatial distributions of water erosion and
80 sediment delivery in the catchment upstream of the Miyun Reservoir, and to quantify
81 the contributions of different land use types to the total catchment SY, and then
82 priority regions were given for future implementation of soil conservation practices in
83 the catchment.

84 **Materials and methods**

85 **Study area description**

86 The catchment upstream of the Miyun Reservoir is located in the northeast of Beijing
87 city. Chaohe River and Baihe River are the two major tributaries that drain into the
88 reservoir (Fig. 1). The catchment covers an area of 15331 km^2, with elevation ranging

89 from 65 to 2300 m a.s.l. Steep slope characterizes the study area, with a mean slope
90 gradient of 34%. The areas with slope gradients above 26.8% and 46.6% occupy
91 around 26% and 56% of the total, respectively.

92 **Fig. 1 is about here**

93 The region has a warm and continental monsoon climate. The mean annual
94 precipitation is around 490 mm, 80% of which falls in summer period. The major
95 soils are Calcic Luvisols, Calcaric Cambisols, Haplic Luvisols, and Haplic
96 Chernozems, with areas occupying 27.6%, 25.1%, 20.3%, and 7.2% of the total,
97 respectively.

98 The main land use types are forest and grass, occupying 63.3% and 22.3% of the
99 total area respectively (Fig. 1). Forest, shrub, and grass are mainly distributed in
100 high-elevation and steep areas. Farmland occupies around 10%, and is mainly
101 distributed in gentle slope areas along the rivers (Fig. 2).

102 **Fig. 2 is about here**

103 Since the 1980s, more and more lands have been widely implemented with soil
104 conservation measures (Li and Li 2008), including terrace, strip ridging, fish-scale pit
105 which are mainly implemented in farmland and orchard field (Fig. 3cd). Compared to
106 the years before 2000, the catchment SY in recent years is much lower (Li and Li,
107 2008). However, there is still over ten thousand tons of sediment entering the
108 reservoir per year. For example, the mean annual SY in 2006-2016 at Xiahui station,
109 the outlet of the Chaohe River, was 0.127×10^4 t, and that at the Zhangjiafen station,
110 the outlet of the Baihe River, was 1.154×10^4 t (Table 1; Fig. 1). The total annual SY

111 entering the reservoir reached 1.284×10^4 t.

112 **Fig. 3 is about here**

113 **Data sources**

114 The RUSLE was used to estimate water erosion. To run this model, datasets including
115 a Digital Elevation Model (DEM), the land use map in 2015, precipitation amount,
116 land use management and soil conservation measures were obtained from different
117 sources.

118 The DEM was downloaded from Shuttle Radar Topography Mission (SRTM)
119 website. After projected with WGS 1984 N52, the resolution in the study area was 27
120 m.

121 The land use data in 2015 was downloaded from the website
122 (http://data.ess.tsinghua.edu.cn/fromglc2017v1.html) by the research team of Gong
123 Peng in Tsinghua University. The data has a 24.5 m resolution in the study area. This
124 high-resolution data can well distinguish different land use types. The data accuracy
125 has been verified by Gong et al. (2020).

126 The daily precipitation data in 2006-2016 at the 50 meteorological stations in the
127 catchment were acquired from the National Climate Centre of Chinese Meteorological
128 Administration (http://data.cma.cn/) and the Annual Hydrological Report of the
129 People's Republic of China.

130 The Harmonized World Soil Database (HWSD) Version 1.2 was obtained from
131 Food and Agriculture Organization of the United Nations (FAO-UN;
132 http://www.fao.org). Soil properties including sand, clay and silt, depth of soil,

133 organic carbon are available from the HWSD.

134 In the current study, due to the high-resolution land use data, all the data
135 mentioned above were resampled using the nearest neighborhood method to a 25-m
136 resolution.

137 During 2006-2016, daily sediment concentration and water level were monitored
138 at eight hydrologic stations (Fig. 1; Table 1). Water discharge (Q) was obtained by
139 using previously established Q-water level curve. Daily SY were then obtained by
140 multiplying sediment concentration and Q (Fang 2019). Annual SY were summed by
141 the daily SY (Table 1). The measured data has been checked and printed in the Annual
142 Hydrological Report:Hydrological Data of Haihe River Basin.

143 **Table 1 is about here**

144 **Methods**

145 **Field campaigns**

146 In October and December 2019, two field campaigns were carried out. In October,
147 runoff plots in Shixia subcatchment were investigated (Fig. 1b). The runoff plots were
148 10-m long with different slope gradients and land use types, some of which have been
149 implemented with soil conservation measures (Table 2). After each rainfall, sediment
150 and runoff collected by containers at the lower end of the plots are measured. Annual
151 SY was obtained through summing the event-based SY occurred in a year. In the
152 current study, annual SYs in 2014-2018 from nine runoff plots were used to verify the
153 estimated results by the RUSLE model. The second field campaign in December was
154 to check the accuracy of land use reclassification from Gong et al. (2020) for Beijing

155 hilly regions.

156 **Table 2 is about here**

157 **RUSLE description**

158 In the current study, the RUSLE modeling approach was used to estimate water
159 erosion, which is calculated as the product of six factors:

160 $$E = R * K * LS * C * P \quad (1)$$

161 where E is the soil erosion intensity (SEI; t ha^{-1} yr^{-1}), R is the rainfall-runoff erosivity
162 factor (MJ mm ha^{-1} h^{-1}), K is the soil erodibility factor (t ha h ha^{-1} MJ^{-1} mm^{-1}), LS is a
163 combination of slope length L and slope gradient S factor (-), C is the crop/cover
164 management factor (-), and P is the soil conservation factor (-).

165 ***R factor***

166 The method to estimate R factor has been significantly improved over that in the
167 original USLE approach. Except for the method proposed by Wischmeier and Smith
168 (1978), alternative methods have widely been used to estimate R-factor value by
169 using different time resolution data (Jiao et al. 2009; Lee et al. 2011). In the current
170 study, the daily precipitation data in 1980-2016 was used to estimate R-factor values,
171 using the method proposed by Zhang et al. (2003):

172 $$R_i = a\sum_{j=1}^{k}(D_j)^b \quad (2)$$

173 Where R_i is the half-month R-factor (MJ mm ha^{-1} h^{-1} yr^{-1}), and D_j is the erosive
174 rainfall day j. D_j is equal to actual rainfall when it is greater than 12 mm. Otherwise it
175 equal to zero. Here, *a* and *b* are empirical parameters. Detailed description was given
176 by Fang and Sun (2017). A Co-Kriging interpolation was used to derive an R-factor

177 value map in ArcGIS 10.5 software. The mean annual R value in 2006-2016 ranged
178 from 1222 to 4749 MJ mm ha^{-1} h^{-1} yr^{-1}, with an average of 2802 MJ mm ha^{-1} h^{-1} yr^{-1}
179 in the study catchment (Fig. 4a).

180 **Fig. 4 is about here**

181 ***K factor***

182 The K factor reflects soil erodibility as affected by intrinsic soil properties. In the
183 current study, soil texture and soil organic carbon content on the top of 30 cm soil
184 layer were extracted from the HWSD. The values of K factor were calculated using
185 the EPIC approach which has been verified in the study area (Liu et al. 2010):

186 $$K = 0.2 + 0.3e^{[-0.0256SAN(1-SIL/100)]} * (\frac{SIL}{CLA+SIL})^{0.3} * \left[1 - \frac{0.25SC}{SC + e^{(3.72-2.95SC)}}\right] * \left[1 - \frac{0.72SN}{SN + e^{(22.9SN-5.51)}}\right] \quad (3)$$

187 where *SAN* is the sand content (%), *SIL* is the silt content (%), *CLA* is the clay content
188 (%), *SC* is the soil organic carbon content (%) and *SN* = 1-*SAN*/100. A soil erodibility
189 map was thus obtained, with K-factor values ranging from 0 to 0.064 t ha h MJ^{-1} mm^{-1}
190 ha^{-1} in the study catchment (Fig. 4b).

191 ***LS factors***

192 The L and S factors represent the effect of topography on water erosion. A 2D
193 approach was used to calculate L factor using the method proposed by Desmet and
194 Govers (1996). The formula by McCool et al. (1989) was used to calculate S factor.

195 $$L_{ij} = \frac{(A_{i,j}+D^2)^{m+1} - A_{i,j}^{m+1}}{D^{m+2} * x_{i,j}^{m} * 22.13^{m}} \quad (4)$$

196 $$x_{i,j} = sin\alpha_{i,j} + cos\alpha_{i,j} \quad (5)$$

197 $$\mathrm{m} = \frac{\beta}{(1+\beta)} \quad (6)$$

$$\beta = \frac{(sin\theta/0.0896)}{[3*(sin\theta)^{0.8}+0.56]} \quad (7)$$

$$S = \begin{cases} 10.8sin\theta + 0.03, \theta < 9\% \\ 16.8sin\theta - 0.5, \theta \geq 9\% \end{cases} \quad (8)$$

where $L_{i,j}$ is the slope length factor of the grid cell with coordinates i and j, $A_{i,j}$ is the contribution area at the inlet of a pixel (m^2), D is the grid cell size (m); $\alpha_{i,j}$ is the slope aspect direction for a pixel; m is slope length exponent, β is empirical factor (-), and θ is the slope angle. The calculated values of LS factor varied from 0.03 to 196.17, with an average of 5.01. Higher LS values occurred in mountainous regions, and lower values appeared along the valleys (Fig. 4c).

C factor

The C factor represents the impact of cropping and management practices on water erosion. In the study area, C-factor values for the land use types were obtained from the published literatures (Bi et al. 2006; Fu et al. 2006; Liu et al. 2010; Fang and Sun 2017; Zerihun et al. 2018; Devátý, et al. 2019; Jazouli et al. 2019). The largest C value was assigned to farmland, followed by orchard and wetland C values of 0.36 and 0.18, respectively (Table 3). The lowest C value of 0.001 was assigned to the forest land (Fig. 4d).

Table 3 is about here

P factor

Because extensive terrace and fit-scale practices have been implemented on farmland and in orchard field, an average value of P factor was set to 0.01 for the farmland, and a value 0.69 was given to the orchard field. The P values of other land use types were set to one (Table 3). The P map was illustrated in Fig. 4e.

SEDD description and calibration

The SEDD model was used to estimate cell SDR_i:

$$SDR_i = e^{-\beta t_i} \quad (9)$$

$$t_i = \sum_{i=1}^{N_p} \frac{l_i}{v_i} \quad (10)$$

where β is a catchment-specific parameter, and t_i is travel time of the eroded soils from the i cell to the nearest stream. It was calculated with the D8 distance to the channels using the TauDEM 5.3.7 module in ArcGIS software (Tarboton 2014). Np is the number of cells along a flow path to the nearest stream, and v_i is the flow velocity passing a cell, which can be obtained using the following equation:

$$v_j = k\sqrt{s_j} \quad (11)$$

where s_j is a cell's slope in gradient (m m^{-1}), and k is the surface roughness coefficient for a cell, and is expressed by sediment water velocity passing a type of land use (m s^{-1}). In the current study, k values of different land use types were from published papers (Table 4). To ensure the proper use of Eq. (10), a minimum cell slope was set to 0.3%, as proposed by Fu et al. (2006).

Table 4 is about here

The parameter β depends primarily on catchment geomorphology, and can be calculated with various candidates. A sensitive analysis is usually used to obtain an appropriate β value. For example, Yang et al. (2012) estimated a β value by changing its values from 4 to 5 with an increment of 0.1. Jain and Kothyari (2000) used this method to estimate β. An inverse modeling approach was also used (e.g., Fernandez et al. 2003; Stefano and Ferro 2007) to estimate β when a mean SDR of a

242 catchment (SDRw) is known by field data or through developed relationships between
243 SDRw and some catchment variables (e.g., Ferro and Porto 2000; Porto et al. 2011).

244 The catchment SY at Yunzhou hydrological station in 2006-2016 was zero
245 because all the sediments were trapped by the Yunzhou reservoir. Similarly, zero SY
246 also occurred at Baihebao hydrological station due to reservoir interception (Fig. 1).
247 Therefore, only the SYs from other six hydrological stations in Table 1 were used to
248 estimate β values. Because SY was zero at Yunzhou hydrological station, its
249 controlled catchment area was deducted from that controlled by Xiabao hydrological
250 station when the SEDD model parameters were calibrated. Similar treatment was also
251 done when the SY at Zhanjiafen hydrological station was used to calibrate the model
252 (Table 1).

253 The calibration procedure was similar to the methods by Fu et al. (2006) and
254 Batista et al. (2017). A series of β values were tested for each catchment, and the
255 estimated SYs were compared with the measured ones. The best fit value of β was
256 obtained when the lowest error occurred. For example, the β values ranging from
257 0.05 to 4.50 were tested with an increment of 0.01 for Gubeikou catchment.
258 Ultimately, the values of β for the six subcatchments controlled by Xiabao,
259 Sandaoying, Zhangjiafen, Dage, Gubeikou, and Xiahui hydrological stations were
260 obtained (Table 5).

261 **Table 5 is about here**

262 The spatial distributed cell SDR_i of the catchments was obtained using Eq.(9),
263 and then cell specific sediment yield (SSY_i) was calculated based on the RUSLE

model:

$$SSY_i = E_i * SDR_i \quad (13)$$

where E_i is the SEI , and the SY of a given catchment was obtained by multiplying the mean SSY_i of the catchment and its area (km^2).

Indexes of topography and geomorphology

Because the β parameter depends mainly on morphologic data (Ferro and Minacapilli, 1995; Ferro et al. 2003), 12 indexes of topography and geomorphology were extracted from the DEM data for the six subcatchments (Table 1). These indexes include catchment area (A), catchment length (CL), relief difference (RD), the ratio of relief difference to catchment length (RD/CL), RUSLE-LS, the mean slope gradient of the river networks (MSR), the total river length (TRL), stream power index (SPI), drainage density (DD), plan curvature (PC), convergence index (CI), and topographic wetness index (TWI). Ferro (1997) concluded that some properties describing the geomorphology and the river networks greatly affected sediment transport efficiency. These indexes were then used to estimate a β value for the study catchment (Table 5).

Sediment trap efficiencies of the reservoirs

There are multiple methods to estimate a reservoir's sediment trap efficiency (STE). In the study catchment above the Miyiun Reservoir, there are two large reservoirs named Yunzhou and Baihebao which are located on the Baihe River (Fig. 1). In 2006-2016, the SYs were zero at the Yunzhou and Baihebao hydrological stations which are located at the outlets of the reservoirs, implying that their STEs were 100%.

There are also many smaller reservoirs or ponds in the catchment (Li, 2007), however, their STEs were not obtained due to unavailable data in the current study.

Results

Soil erosion

The mean annual SEI of the catchment upstream of the Miyun Reservoir ranged from 0 to 902 t ha^{-1} yr^{-1}, with an average of 4.08 t ha^{-1} yr^{-1} (Fig. 5). It was over two times the soil loss tolerance (T=2.00 t ha^{-1} yr^{-1}) in the study area (Hua et al. 2005). Around 62% of the cells had SEI less than one T. The area percentages of the cell SEIs with 2-5, 5-10, 10-15, 15-25, and 25-50 t ha^{-1} yr^{-1} were around 6.15%, 8.46%, 7.13%, 9.27%, and 6.3% respectively. The area percentage with SEI higher than 50 t ha^{-1} yr^{-1} was less than 1.0%.

Soil loss widely occurred in the catchment, and varied greatly. Higher SEI mainly appeared in the areas along the channels (Fig. 5). Considering the drainage area (15331 km^2) of the catchment, annual total soil loss reached 6,255,048 tons.

Fig. 5 is about here

Calibrated β

The calibration using the SYs from the 6 subcatchments (i.e., catchments controlled by Dage, Gubeikou, Xiahui, Sandaoying, Xiabao, and Zhangjiafen hydrological stations) yielded different β values, ranging from 0.04 in Dage subcatchment to 4.00 in Xiahui subcatchment (Fig. 1). Pearson correlation matrix showed that these β values were significantly correlated with A, CL, FD, and SPI at the 0.01 significance level, and FD/CL, PC at the 0.05 significance level (Table 6). The β values were

exponentially correlated with FD/CL and CI indexes, and linearly with other indexes. After exponentially conversion of these two indexes, standardization of all the indexes, a stepwise linear regression was established with the F probability with entry of 0.05 and removal of 0.1, yielding a regression equation:

$$\beta = 0.961 CL_* \quad R^2 = 0.924 \qquad (14)$$

where CL_* is the standardized CL. According to this equation, a β value of 1.73 for the catchment upstream of the Miyun Reservoir was obtained, considering a standardized CL_* value of 1.797 for the whole catchment.

Table 6 is about here

SDR and SSY

A spatially distributed map of SDR_i in the catchment upstream of the Miyun Reservoir was obtained using Eq. (9) with the estimated β value of 1.73 (Fig. 6a). The values of cell SDR_i ranged from 0 to 100%, with an average of 1.65%, and a standard deviation of 12.69%. Around 98% cells had an SDR_i less than unit. Spatially, the SDR_i showed a network distribution pattern. The farther away from the river networks, the smaller the SDR_i values were.

The mean SSY_i of the catchment ranged from zero to 902 t ha^{-1} yr^{-1}, with an average of 0.04 t ha^{-1} yr^{-1} (Fig. 6b). The distance to streams greatly influenced SSYi. The spatial distribution pattern of the cell SSY_i was quite similar to that of the SDR_i, resulting from significant modification of SEI_i by SDR_i. Around 68% of the cells had zero value, indicating that most of the eroded sediment cannot reach channels. The cells with 0-2 t ha^{-1} yr^{-1} occupied 30% of the total. The total annual SY of the

catchment was 6.90×10^4 t.

Fig. 6 is about here

Discussion

Model performance

This study uses RUSLE and SEDD models to estimate soil erosion and sediment delivery in the catchment upstream of the Miyun Reservoir. Therefore, their performance should be verified. In the study area, soil erosion has been studied using the RUSLE model (Zhou and Wu 2008; Feng et al. 2019), tracer method (Hua et al. 2005), and runoff plots (Table 7). In the current study, the estimated SEIs were 1.66 and 13.36 t ha^{-1} yr^{-1} on forest and grass lands. Such values are in agreement with the counterparts by Feng et al. (2019), which are 2.01 and 1.90 t ha^{-1} yr^{-1} on forest and grass lands, respectively. In contrast, the estimated SEI on the forest land was lower than that (i.e., 26.36 t ha^{-1} yr^{-1}) by Hua et al. (2005). However, the estimated SEI of 20.84 t ha^{-1} yr^{-1} on shrub land in the current study coincided well with that (i.e.,17.30 t ha^{-1} yr^{-1}) by Hua et al. (2005).

In respect of SEI on farmland, the estimated SEI of 6.15 t ha^{-1} yr^{-1} is much higher than that (i.e., 0.10 t ha^{-1} yr^{-1}) on runoff plot. Similarly, the estimated SEIs on other types of lands are also higher than the counterparts on the runoff plots (Table 2). This could be due to lower slope length and slope gradient of the plots. This hypothesis can to some extent be verified that the SEI on the 14.4° runoff plot with contour cultivation is much higher than the estimated one in the current study.

Factors influencing water erosion are multiple, and methods used also greatly

352 influence the results. Thus, differences between our results and others are acceptable
353 (Fang and Sun 2017).

354 The simulated SYs for the six subcatchments were compared to the measured
355 ones in Table 1. As expected, the SSYs in smaller subcatchments (i.e., SY at Dage,
356 Xiabao, and Sanyimiao) were underestimated, and verse visa (Fig. 7). However, the
357 Adjusted R^2 of the fitting line reaches 0.64, resulting from the compromise of
358 parameter calibration for different catchments.

359 **Fig. 7 is about here**

360 **Impact of land use**

361 The distribution of soil loss is greatly influenced by land use types (e.g., Ranzi et al.
362 2012; Naqvi et al. 2019). The distribution pattern of SEI was quite similar to that of
363 the grassland because the grassland was widely distributed in the catchments with
364 higher SEI of 13.36 t ha^{-1} yr^{-1}. As a result, the SY from grass land contributed nearly
365 70% to the total.

366 Although farmland was widely implemented with soil conservation measures, it
367 occupied only 3.95% of the study area. The SY from the farmland occupied nearly 17%
368 of the total, which was the second sediment contributor to the catchment. In contrast,
369 forest area occupied near 64% of the total area, whereas its SY contribution to the
370 total was less than 7%, resulting from smaller SEI (i.e., 1.66 t ha^{-1} yr^{-1}) and SDR (i.e.,
371 0.72%). In the study area, bare land suffered the highest SEI (i.e., 39.1 t ha^{-1} yr^{-1}) and
372 higher SDR (Table 7). This result coincided with published studies. For example, in
373 the Isábena catchment of southern central Pyrenees, most sediments came from the

374 bare land although its area percentage was less than 1% (López-Tarazón et al. 2009).
375 The highest SEI was also observed in the upper Grande River catchment, Brazil
376 (Batista et al. 2017). Therefore, bare land should be the priority area for future soil
377 loss control. Orchard land also had much higher SEI (i.e., 17.73 t ha^{-1} yr^{-1}) with the
378 largest SDR. However, because its area percentage was much less, its contribution to
379 the total SY only occupied 0.02%. This type of land should also be paid attention to
380 because soil loss from orchard field could lead to severe water pollution in the study
381 area (Liu et al. 2003).

382 **Table 7 is about here**

383 **Impact of topography**

384 Both SEI and sediment delivery were greatly influenced by topography. Steeper
385 slopes usually had higher values of LS factor (Vijith et al. 2018), resulting in higher
386 SEI (Fig. 8ab). However, a threshold value of SSY occurred on the 3-5 degree slopes.
387 On the gentle slopes, sediment does not easily enter the steams. However, sediment
388 flow on steeper slopes usually requires a long distance to reach streams, resulting in a
389 less SSY. Their interaction can thus produce a threshold value of SSY with increasing
390 slope gradients.

391 **Fig. 8 is about here**

392 With respect to the impact of elevation on soil erosion and sediment delivery,
393 both SEI and SSY presented decreasing trends with the largest values occurred in the
394 200-300 m a.s.l regions (Fig. 8). The RUSLE-derived soil erosion map apparently
395 indicated higher SEI in this elevation range (Fig. 5). This could result from extensive

396 land reclamation in lower elevation areas in recent years (Pang et al. 2010; Feng et al.
397 2019).

398 Noticeably, forest, grass, and shrub lands were mainly distributed in in the steep
399 areas with higher elevations (Fig. 2), where the rates of soil loss were lower on the
400 forest and shrub lands, while higher SEI on the grass land (Table 6). The bare land
401 which had the largest SEI is mainly distributed in the areas above 1000 m a.s.l. Soil
402 loss control for these two types of lands also should be done.

403 **Uncertainty analyses**

404 The β parameter is a major source of uncertainty in the SEDD model (Batista et al.
405 2017). The published β values differed greatly in literature, varying from 0.2 h^{-1}
406 (Yan et al. 2018), 1.0 h^{-1} (Fu et al. 2006), 3.0 h^{-1} (Batista et al. 2017), to 4.6 h^{-1} (Yang
407 et al. 2012), respectively. The β mainly depends on catchment geomorphology. It
408 usually increases with increasing catchment area A (Ferro and Minacapilli 1995;
409 Batista et al. 2017). In the study area, it is not only positively correlated with A at the
410 significance of 0.01 level, but also correlated with other geomorphologic indexes
411 (Table 6). This means larger catchment size doesn't necessarily yield a large β value.
412 The current study verifies this inference. The derived β value of 1.73 from the
413 stepwise regression equation Eq. (14) is smaller than those from Zhanjiafen,
414 Gubeikou, and Xiahui catchments, and higher than those from other smaller
415 catchments (Table 1). Batista et al. (2017) also pointed that although the β generally
416 increases with increasing catchment size, the relation may not be straight-forward.
417 The determined coefficient R^2 reached 0.64, indicating the estimated β was

418 acceptable.

419 The combined use of RUSLE and SEDD models generated around 6.90×10^4
420 tons of sediment for the study catchment. This value is much higher than the summed
421 SY (1.281×10^4 t) monitored at the Zhanjiafen and Xiahui stations on the Baihe and
422 Chaohe River outlets, respectively. The deviation could be explained by at least two
423 aspects. In the study area, there were many dams or reservoirs, including the two
424 largest ones named Yunzhou and Baihebao reservoirs on the Baihe River (Fig. 1).
425 Much of the eroded sediment from catchment upstream is trapped by the reservoirs.
426 For example, there was no sediment flowed out of the Yunzhou and Baihebao
427 reservoirs in 2006-2016. This means that all the sediments from the upstream areas
428 were trapped by these two reservoirs. The estimated annual SYs of 0.73×10^4 and
429 2.81×10^4 were trapped within the Yunzhou and Baihebao reservoirs, which occupied
430 11% and 41% of total SY. Many other reservoirs and dams exist in the study
431 catchment (Li 2007), and a lot of sediment would be trapped in the reservoirs.

432 The study catchment has an area of 15, 331 km^2 with zigzagged channels in the
433 downstream areas (Fig. 1). As a result, more sediment is deposited on the flood plains
434 (Bai et al. 2018; Zhang et al. 2019). However, sediment deposition is not considered
435 in the SEDD, and the data of deposited sediment in channels are also unavailable. In
436 the SEDD model, all the sediments from the upper slopes were directly routed out of
437 the catchment, without considering sediment behavior in channels (Batista et al.
438 2017).

439 Therefore, the employment of the sediment data just from hydrological stations

could be biased, and more sediment information in channels should be explored and considered. Future version of SEDD that envelopes sediment suspension and deposition modules in channels could greatly improve its simulation accuracy.

Conclusions

Spatial distributions of water erosion and sediment delivery were explicated by using RUSLE and SEDD models for the catchment upstream of the Miyun Reservoir, and sediment sources areas were was recognized in the current study.

In the catchment, bare land suffered the highest SEI of 39.01 t ha^{-1} yr^{-1}. Higher SEIs also occurred on the shrub land, orchard field, and grass land. Orchard field had the highest SDR of 10.35%, but its contribution of SY was less due to its less area percentage. The SY mainly came from grass land and farmland, occupying around 70% and 17% of the total, respectively. Soil conservation practices should focus on these lands to further control soil loss, especially those located in the regions with 3 to 5° slopes and/or elevations less than 500 m a.s.l.

Because no specific field data of sedimentation in the river networks, dams and/or reservoirs in the catchment, the estimated β value could under- and over-estimate sediment delivery over the catchment. A model with sediment suspension and deposition modules in channels could better elucidate sediment delivery of the catchment when more robust field data are available. However, the combination of RUSLE and SEDD can still help explicate the major sediment source and guide future implementation of soil conservation measures in the Beijing hilly regions.

462 **Acknowledgments**

463 This work was financially supported by projects of Beijing Municipal Natural Science

464 Foundation (grant number 8202045), and the National Natural Science Foundation of

465 China (grant number 41977066).

466

467

468 **References**

469 Bai XD, Zhang Y, Guan CY, Yuan SH, Lu LN, Ma XD, Li KY (2018) Grain size analysis of the
470 late Pleistocene-Early Holocene sediment in the lower Chaobai River. Sci Tech Engi 18(17*)*:
471 1671-1815.

472 Batista PVG, Silva MLN, Silva BPC, Curi N, Bueno IT, Junior FWA, Davies J (2017) Modelling
473 spatially distributed soil losses and sediment yield in the upper Grande River Basin- Brazil.
474 Catena, 157: 139-150. https://doi.org/10.1016/j.catena.2017.05.025.

475 Bi XG, Duan SH, Li YG, Liu BY, Fu SH, Ye ZH, Yuan AP, Lu BJ (2006) Study on soil loss
476 equation in Beijing. Sci Soil Water Conserv 4(4): 6-13.

477 Desmet P, Govers G (1996) A GIS procedure for automatically calculating the USLE LS factor on
478 topographically complex landscape units. J Soil Water Conserv 51: 427-433.

479 Devátý J, Dostál T, Hösl R, Krása J, Strauss P (2019) Effects of historical land use and land
480 pattern changes on soil erosion – Casestudies from Lower Austria and Central Bohemia.
481 Land Use Policy, 82: 674-685. https://doi.org/10.1016/j.landusepol.2018.11.058.

482 Fang HY (2019) Temporal changes in suspended sediment transport during the past five decades
483 in a mountainous catchment, eastern China. J Soil Sedi 19: 4073-4085.
484 https://doi.org/10.1007/s11368-019-02363-x.

485 Fang HY, Sun LY (2017) Modelling soil erosion and its response to the soil conservation
486 measures in the black soil catchment, Northeastern China. Soil Till Res 165: 23-33.
487 http://dx.doi.org/10.1016/j.still.2016.07.015.

488 Feng JJ, Shi MC, Jiang QO (2019) Influence of land use /cover change on soil erosion in Chaobai
489 River Basin. Sci Soil Water Conserv 17(3): 121-132.

490 Fernandez C, Wu JQ, Mccool DK, Stockle CO (2003) Estimating water erosion and sediment

yield with GIS, RUSLE, and SEDD. J Soil Water Conserv 58: 128-136

Ferro V (1997) Further remarks on a distributed approach to sediment delivery. Hydro Sci J 42(5): 633-647. https://doi.org/10.1080/02626669709492063.

Ferro V, Minacapilli M (1995) Sediment delivery processes at the basin scale. Hydro Sci J 40(6): 703-717. https://doi.org/10.1080/02626669509491460.

Ferro V, Porto P (2000) Sediment delivery distributed (SEDD) model. J Hydro Engi 5: 411-422. https://doi.org/10.1061/(ASCE)1084-0699(2000)5:4(411).

Ferro V, Stefano CD, Minacapilli M (2003) Calibrating the SEDD model for Sicilian ungauged basins. Int As Hydr Sci Pub 279: 151-161. http://dx.doi.org/.

Ferro V, Porto P (2000) Sediment delivery distributed (Sedd) model. J Hydr Engi 5: 411-422. https://doi.org/10.1061/(ASCE)1084-0699(2000)5:4(411).

Fu GB, Chen SL, McCool DK (2006) Modeling the impacts of no-till practice on soil erosion and sediment yield with RUSLE, SEDD, and ArcView GIS. Soil Till Res 85: 38-49. https://doi.org/10.1016/j.still.2004.11.009.

Fu SH, Wu JD, Duan SH, Li YG, Liu BY (2001). Effect of soil and water conservation practice on soil erosion at Shixia Watershed. J Soil Water Conserv 15(2): 21-24.

Gong P, Li XC, Wang J, Bai YQ, Chen B, Hu TY, Liu XP, Xu B, Yang J, Zhang W, Zhou YY (2020) Annual maps of global artificial impervious area (GAIA) between 1985 and 2018. Remote Sens Environ 236: 111510. https://doi.org/10.1016/j.rse.2019.111510.

Guo QK, Ding ZW, Qin W, Cao WH, Lu W, Xu XM, Yin Z (2019) Changes in sediment load in a typical watershed in the tableland and gully region of the Loess Plateau, China. Catena 182: 104132. https://doi.org/10.1016/j.catena.2019.104132.

513 Hua L, Zhang ZG, Li JB, Feng Y, Zhao H, Yin XX, Zhu FY (2005) Soil erosion and organic
514 matter loss by using fallout ^{137}Cs as tracer in Miyun Reservoir valley. Acta Agri Nucl Sinica,
515 19: 208-213.
516 Jain MK, Kothyari UC (2000) Estimation of soil erosion and sediment yield using GIS. Hydr Sci J:
517 45: 771-786. https://doi.org/10.1080/02626660009492376.
518 Jazouli AE, Barakat A, Khellouk R, Rais J, Baghdadi ME (2019) Remote sensing and GIS
519 techniques for prediction of land use land cover change effects on soil erosion in the high
520 basin of the OumErRbia River (Morocco). Remote Sens Appli: Soc Environ 13: 361-374.
521 https://doi.org/10.1016/j.rsase.2018.12.004.
522 Jiao J, Xie Y, Lin Y, Zhao DF (2009) Study on rainfall-runoff erosivity index in Northeastern
523 China. *Sci Soil Water Conserv 7(3)*: 6-11.
524 Lee, J.K., Heo, J.H. (2011). Evaluation of estimation methods for rainfall erosivity based on
525 annual precipitation in Korea. J Hydr 409: 30-48.
526 https://doi.org/10.1016/j.jhydrol.2011.07.031.
527 Li ZJ, Li XB (2008) Impacts bf Engineering Measures for Water Conservancy on annual runoff in
528 the Chaohe River basin based on an empirical statistical model. Acta Geogra Sinica 63(9):
529 958-968.
530 Liu BY, Bi XG, Fu SH (2010) Beijing Soil Loss Equation. Beijing: Science Press.
531 Liu HW, Yu S (2018) Spatio-temporal variational characteristics analysis of heavy metals
532 pollution in water of the typical northern rivers, China. J Hydr 559: 787-793.
533 https://doi.org/10.1016/j.jhydrol.2018.02.081.
534 Liu SH, Yu XX, Hu CH, Gao GX (2003) Nutrient cycling in Chestnut field in the Miiyun

Reservoir watershed, Beijing. Chin. J Appl Ecol 14: 1597-1601.

López-Tarazón JA, Batalla RJ, Vericat D, Francke T (2009) Suspended sediment transport in a highly erodible catchment: The River Isábena (Southern Pyrenees). Geomorphology 109: 210-221. https://doi.org/10.1016/j.geomorph.2009.03.003.

McCool, D.K., Foster, G.R., Mutchler, C., Meyer, L. (1989). Revised slope length factor for the universal soil loss equation. Trans Am Soc Agr Engi 32: 1571-1576. https://doi.org/10.13031/2013.30576.

Mehri A, Salmanmahiny A, Tabrizi ARM, Mirkarimi SH, Sadoddin A (2019) Investigation of likely effects of land use planning on reduction of soil erosion rate in river basins: Case study of the Gharesoo River Basin. Catena 167: 116-129. https://doi.org/10.1016/j.catena.2018.04.026.

Modes DW, Kmoch A, Bhat HG, Uuemaa E (2020) Future soil loss in highland Ethiopia under changing climate and land use. Reg Environ Change 20: 32. https://doi.org/10.1007/s10113-020-01617-6.

Naqvi HR, Athick ASMA, Siddiqui L, Siddiqui MA (2019) Multiple modeling to estimate sediment loss and transport capacity employing hourly rainfall and In-Situ data: A prioritization of highland watershed in Awash River basin, Ethiopia. Catena 182: 104173. https://doi.org/10.1016/j.catena.2019.104173.

Pandey A, Himanshu SK, Mishra SK, Singh VP (2016) Physically based soil erosion and sediment yield models revisited. Catena 47: 595-620. https://doi.org/10.1016/j.catena.2016.08.002.

Pang JP, Liu CM, Xu ZX (2010) Impact of land use changes on runoff and sediment yield in the

557 Miyun Reservoir catchment. J Beijing Nor Uni 46: 290-299.
558 Porto P, Walling DE (2015) Use of Caesium-137 measurements and long-term records of sediment
559 load to calibrate the sediment delivery component of the SEDD model and explore scale
560 effect:examples from Southern Italy. J Hydr Engi 20, (C4014005-1-C4014005-12).
561 https://doi.org/10.1061/(ASCE)HE.1943-5584.0001058.
562 Porto P, Walling DE, Callegari G (2011) Using ^{137}Cs measurements to establish catchment
563 sediment budgets and explore scale effects. Hydr Process, 25: 886-900.
564 https://doi.org/10.1002/hyp.7874.
565 Qin W, Guo QK, Cao WH, Yin Z, Yan QH, Shan ZJ, Zheng FL (2018) A new RUSLE slope
566 length factor and its application to soil erosion assessment in a Loess Plateau watershed. Soil
567 Till Res 182: 10-24. https://doi.org/10.1016/j.still.2018.04.004.
568 Ranzi R, Le TH, Rulli MC (2012) A RUSLE approach to model suspended sediment load in the
569 Lo River (Vietnam): Effects of reservoirs and land use changes. J Hydr 422-423: 17-29.
570 https://doi.org/10.1016/j.jhydrol.2011.12.009.
571 Rickson RJ (2014) Can control of soil erosion mitigate water pollution by sediments? Sci Tot
572 Environ 468-469: 1187-1197. https://doi.org/10.1016/j.scitotenv.2013.05.057.
573 Di Stefano C, Ferro V (2007) Evaluation of the SEDD model for predicting sediment yield at the
574 Sicilian experimental SPA2 basin. Earth Surf Process Landf 32:
575 1094-1109. https://doi.org/10.1002/esp.1465.
576 Tang LH, Yang DW, Hu HP, Gao B (2011) Detecting the effect of land-use change on streamflow,
577 sediment and nutrient losses by distributed hydrological simulation. J Hydr 409: 172-182.
578 https://doi.org/10.1016/j.jhydrol. 2011.08.015.

579 Tarboton DG (2014) TauDem 5.3.7: terrain analysis using digital elevation models. Available
580 in:http://hydrology.usu.edu/taudem/taudem5/downloads.html.
581 Vercruysse K, Grabowsk IR, Rickson RJ (2017) Suspended sediment transport dynamics in rivers:
582 multi-scale drivers of temporal variation. Earth-Sci Rev 166: 38-52.
583 https://doi.org/10.1016/j.earscirev.2016.12.016.
584 Vijith H, Hurmain A, Dodge-Wan D (2018) Impacts of land use changes and land cover alteration
585 on soil erosion rates and vulnerability of tropical mountain ranges in Borneo. Remote Sens
586 Appli: Soc Enviro 12: 57-69. https://doi.org/10.1016/j.rsase.2018.09.003.
587 Walling DE, Owens PN, Leeks GJL (1999) Fingerprinting suspended sediment sources in the
588 catchment of the River Ouse, Yorkshire, UK. Hydr Process 13, 955-975.
589 https://doi.org/10.3390/w10111573.
590 Wilkinson SN, Prosser IP, Rustomji P, Read AM (2009) Modelling and testing spatially distributed
591 sediment budgets to relate erosion processes to sediment yields. Environ Modeling Soft 24:
592 489-501. https://doi.org/10.1016/j.envsoft.2008.09.006.
593 Wischmeier WH, Smith DD (1978) Predicting Rainfall Erosion Losses: A Guide to Conservation
594 Planning. Agriculture Handbook Number 537. United States Department of Agriculture.
595 Yan R, Zhang XP, Yan SJ, Chen H (2018) Estimating soil erosion response to land use/cover
596 change in a catchment of the Loess Plateau, China. Int Soil Water Conserv Res 6: 13-22.
597 https://doi.org/10.1016/j.iswcr.2017.12.002.
598 Yang M, Li X, Hu Y, He X (2012) Assessing effects of landscape pattern on sediment yield using
599 sediment delivery distributed model and a landscape indicator. Ecol Indi 22: 38-52.
600 https://doi.org/10.1016/j.ecolind.2011.08.023.

601 Zerihun M, Mohammedyasin MS, Sewnet D, Adem AA, Lakew M (2018) Assessment of soil
602 erosion using RUSLE, GIS and remote sensing in NW Ethiopia. Geoderma Reg 12:83-90
603 Zhang J, Ji DL, Bai YN, Miao JJ, Guo X, Du D, Pei YD (2019) Research on the
604 macro-characteristics of the sedimentation in the middle reach of Chaobai River based on
605 remote sensing. Remote Sens Land Res 31: 156-163.
606 Zhang WB, Fu JS (2003) Using different types of rainfall datasets to estimate rainfall erosivity.
607 Res Sci 25(1): 26-28.
608 Zhao GJ, Gao P, Tian P, Sun WY, Hu JF, Mu XM (2020) Assessing sediment connectivity and soil
609 erosion by water in a representative catchment on the Loess Plateau, China. Catena 185:
610 104284. https://doi.org/10.1016/j.catena.2019.104284.
611 Zhou WF, Wu BF (2008) Assessment of soil erosion and sediment delivery ratio using remote
612 sensing and GIS: a case study of upstream Chaobaihe River catchment, north China. Int J
613 Sedi Res 23: 167-173.
614

615 **Table 1** The catchment area, annual mean catchment sediment yield (SY) and area specific SY

616 (SSY) in 2006-2016 controlled by the eight hydrological stations on the Chaohe and Baihe

617 Rivers.

Rivers	Station name	A km^2	SY 10^4 t yr^{-1}	SSY t km^{-2} yr^{-1}
Chaohe	Dage◆	1850	20.057	108.42
	Gubeikou◆	4701	1.906	4.05
	Xiahui◆	5340	0.127	0.24
Baihe	Yunzhou	1170	0.000	0.00
	Xiabao◆	4015	4.632	11.54
	Baihebao	4040	0.000	0.00
	Sandaoying◆	1536	2.302	14.99
	Zhangjiafen◆	8506	1.154	1.36

618 Note:◆indicates the SY used to calibrate SEDD model.

619

620 **Table 2** Land use types, slope gradients, implemented measures, and mean annual SEIs of

621 different runoff plots in the Shixia subcatchment in 2014-2018.

Runoff plot	Land use type	Slope (°)	Measures	Mean annual SEI (t ha^{-1} yr^{-1})
1	Terrace (corn)	3.5	Width:4m	0.10
2	Contour cultivation (corn)	14.4	-	20.92
3	Farmland (corn)	16.5	-	27.31
4	Bare land	16.5	-	26.40
5	Chestnut	16.5	Width:3m，Coverage:50%	1.37
6	Arbor	17.1	Fish-scale pit; 80% coverage	0.04
7	Shrub land	18.6	Coverage:50%	0.22
8	Grassland	19.0	Coverage:80%	0.04
9	Grassland	19.0	Coverage:<30%	2.52

622

623

624

625

626 **Table 3** The values of RUSLE-C and -P factors used in the current study.

Land use type	C	P	Reference
Farmland	0.47	0.1	Bi et al. 2006; Liu et al. 2010
Forest	0.001	1.00	Liu et al. 2010; Zerihun et al. 2018; Devátý, et al. 2019
Orchard	0.23	0.69	Bi et al. 2006; Liu et al. 2010
Shrubland	0.029	1.00	Liu et al. 2010
Grassland	0.033	1.00	Liu et al. 2010
Marshland, wetland	0.18	1.00	Fang and Sun 2017
Water	0	1.00	Fu et al. 2006; Fang and Sun 2017
Impervious surface	0.003	1.00	Fu et al. 2006; Jazouli et al. 2019
8, Bare land	0.181	1	Fang and Sun 2017

627 Note: All the studies in "reference" column were conducted in the NEC.

628
629

630 **Table 4** The values of k (m s^{-1}) in the SEDD model for different land use types (Sources:Ferro and

631 Porto, 2000; Fernandez, et al. 2003; Yan et al. 2018; Batista et al. 2017)

Forest	Shrubland, and orchard	Grassland	Residential land	farmland	Water
0.75	0.75	2.13	5.14	2.62	4.91

632
633
634
635
636
637
638
639
640
641
642

643 **Table 5** Extracted indexes of topography and geomorphology for the subcatchments controlled by

644 the six hydrological stations in Table 1.

	Dage	Gubeikou	Xiahui	Xiabao	Sandaoying	Zhangjiafen
β	0.04	3.82	4.00	0.34	0.21	3.55
A (km^2)	1857	4627	4800	2909	1536	4554
CL (km)	59.74	131.32	141.53	79.38	85.57	118.80
RD (km)	1575	1989	2008	1591	1768	2117
RD/CL (-)	26.36	15.15	14.19	20.04	20.66	17.82
RUSLE-LS	5.07	5.36	5.34	5.29	6.26	6.73
MSR($m\ m^{-1)}$	0.043	0.039	0.039	0.041	0.05	0.05
TRL (km)	523.38	3440.24	3571.60	2140.21	1113.80	3247.18
SPI	29647.55	73779.05	80125.58	34326.97	42240.08	101386.93
DD ($km\ km^{-1}$)	0.28	0.74	0.74	0.74	0.73	0.71
PC($\times 10^3$)	0.18	0.22	0.22	0.19	0.20	0.25
CI /($\times 10^3$)	-0.68	-0.79	-0.86	-0.74	-0.54	-0.76
TWI	6.49	6.46	6.47	6.52	6.32	6.23

645 Note: The abbreviation A, CL, RD, RD/CL, RUSLE-LS, MSR, TRL, SPI, DD, PC, CI, TWI represents catchment

646 area, catchment length, relief difference, the ratio of relief difference to catchment length, RUSLE-LS, the

647 mean slope gradient of river networks, total river length, stream power index, drainage density, plan curvature,

648 convergence index, and topographic wetness index, respectively.

649

650

651

652

653

654

655

656

Table 6 Pearson correlation matrix between β and the 12 indexes of topography and morphology.

	β	A	CL	RD	RD/CL	RUSLE-LS	MSR	TRL	SPI	DD	PC	CI
A	0.960**											
CL	0.961**	0.909*										
RD	0.923**	0.827*	0.902*									
RD/CL	-0.862*	-0.853*	-0.956*	-0.796								
RUSLE-LS	0.179	0.081	0.186	0.531	-0.158							
MSR	-0.269	-0.381	-0.277	0.112	0.316	0.877*						
TRL	0.934**	0.973**	0.940**	0.833*	-0.939*	0.153	-0.336					
SPI	0.920**	0.867*	0.860*	0.978**	-0.748	0.527	0.108	0.849*				
DD	0.476	0.501	0.648	0.541	-0.821*	0.394	0.011	0.685	0.486			
PC	.0.841*	0.788	0.790	0.959**	-0.702	0.667	0.262	0.795	0.981**	0.543		
CI	-0.773	0.886*	-0.698	-0.504	0.647	0.319	0.674	-0.810	-0.587	-0.229	-0.454	
TWI	-0.219	-0.085	0.195	-0.568	0.113	-0.981*	-0.880*	-0.124	-0.588	-0.266	-0.680	-0.315

* Significant at 0.05 level; ** significant at 0.01 level.

662

663 **Table 7** Soil erosion intensity (SEI), SDR, and SY at each land use type.

Land use class	SEI ($t\ ha^{-1}\ yr^{-1}$)	SDR (%)	SSY ($t\ ha^{-1}\ yr^{-1}$)	Area (km^2)		SY	
						$t\ yr^{-1}$	%
1, Farmland	6.14	6.71	0.39	629.50	3.95	24,660	16.86
2, Orchard	17.73	10.35	2.02	0.13	0.00	26	0.02
3, Forest	1.66	0.72	0.01	9207.74	57.83	9361	6.40
4, Grass land	13.36	2.55	0.18	5613.16	35.26	102,033	69.76
5, Shrubland	20.84	1.19	0.16	311.33	1.96	4,892	3.34
6, Water body/wetland	2.08	4.77	0.21	86.83	0.55	1,789	1.22
7, Impervious surface	2.42	5.17	0.09	33.50	0.21	316	0.22
8, Bare land	39.01	4.35	0.82	38.97	0.24	3,195	2.18

664

665

666

667

668

669

670

671 ## Figure captions:

672 **Fig. 1** Maps showing (a) location of the catchment upstream of the Miyun Reservoir, (b) the
673 distributions of hydrological stations, meteorological stations, Shixia subcatchment, reservoirs,
674 and the elevation range, (c) slope gradient, and (d) land use types

675 **Fig. 2** The mean slope gradients and elevations of different land use types distributed in the study
676 catchment. Note:the numbers in the x-axis represent land use types in Table 7

677 **Fig. 3** Pictures showing (a) runoff plot with bare soil, (b) forest, (c) terraced farmland, and (d) tree
678 tray in the orchard field

679 **Fig. 4** Spatial distributions of the values of RUSLE-R, -K, -LS, -C, and -P factors in the study
680 catchment

681 **Fig. 5** Spatial distribution of the estimated soil erosion intensity (SEI) in the study catchment

682 **Fig. 6** Map showing the spatial distributions of the estimated SDR (a) and SSY (b).

683 **Fig. 7** Comparison between the measured SSY with the simulated ones for the six subcatchments
684 in Table 1

685 **Fig. 8** Soil erosion intensity (SEI) and SSY (ac), and RUSLE-LS factor and flow length of the
686 cells to the nearest channels with increasing slope gradients and elevations (bd)

687

688

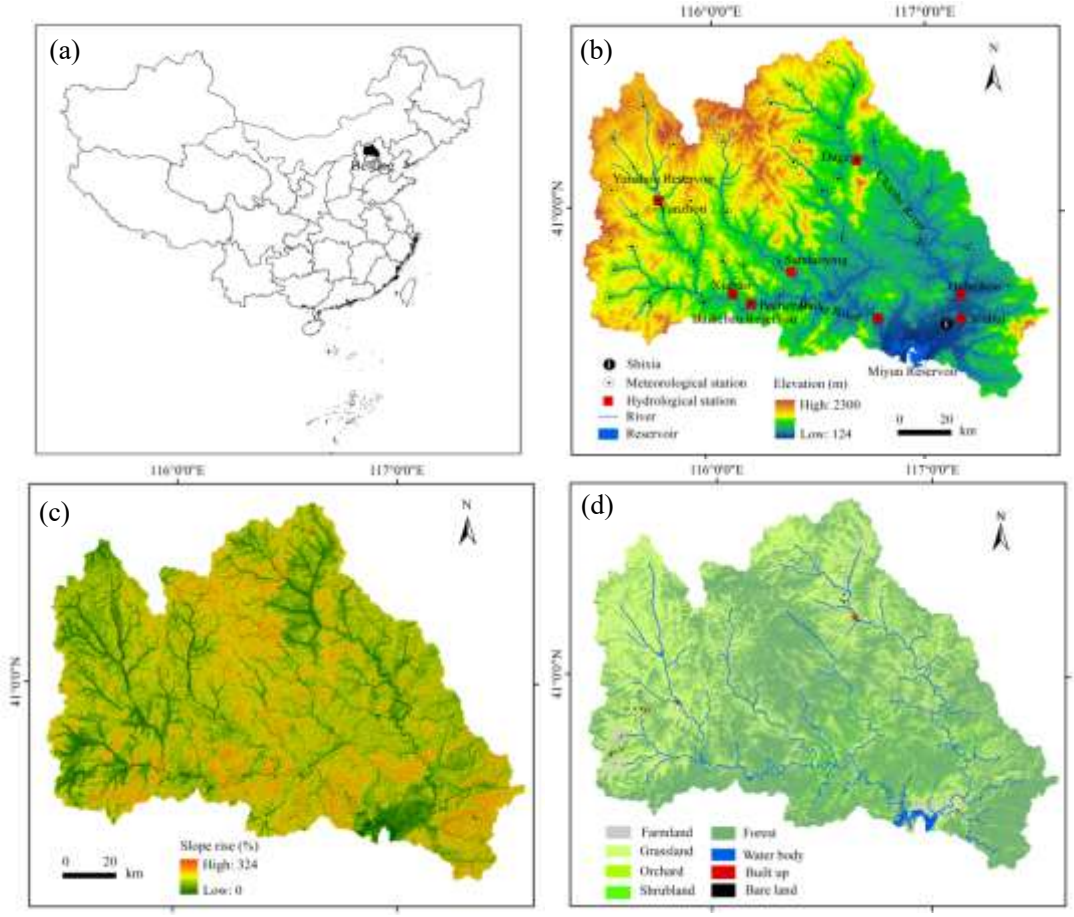

689 **Fig. 1**

690

691

692

693

694

695

696

697

698

699

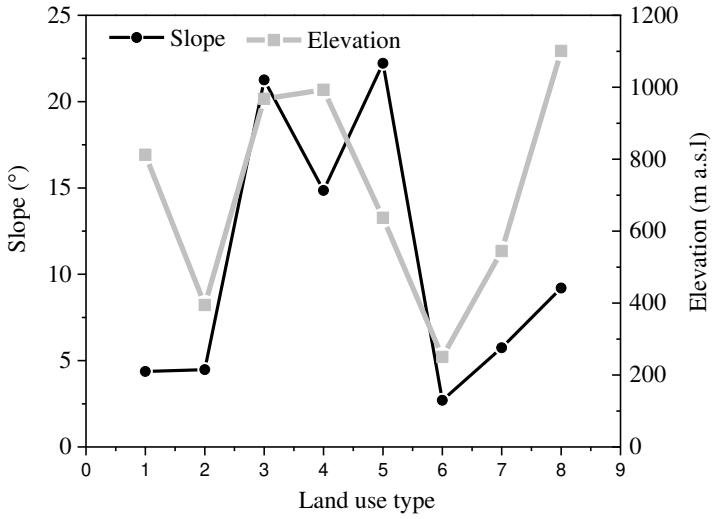
Slope
Elevation
Slope (°)
Elevation (m a.s.l)
Land use type
0
5
10
15
20
25
0
200
400
600
800
1000
1200
0
1
2
3
4
5
6
7
8
9

Fig. 2

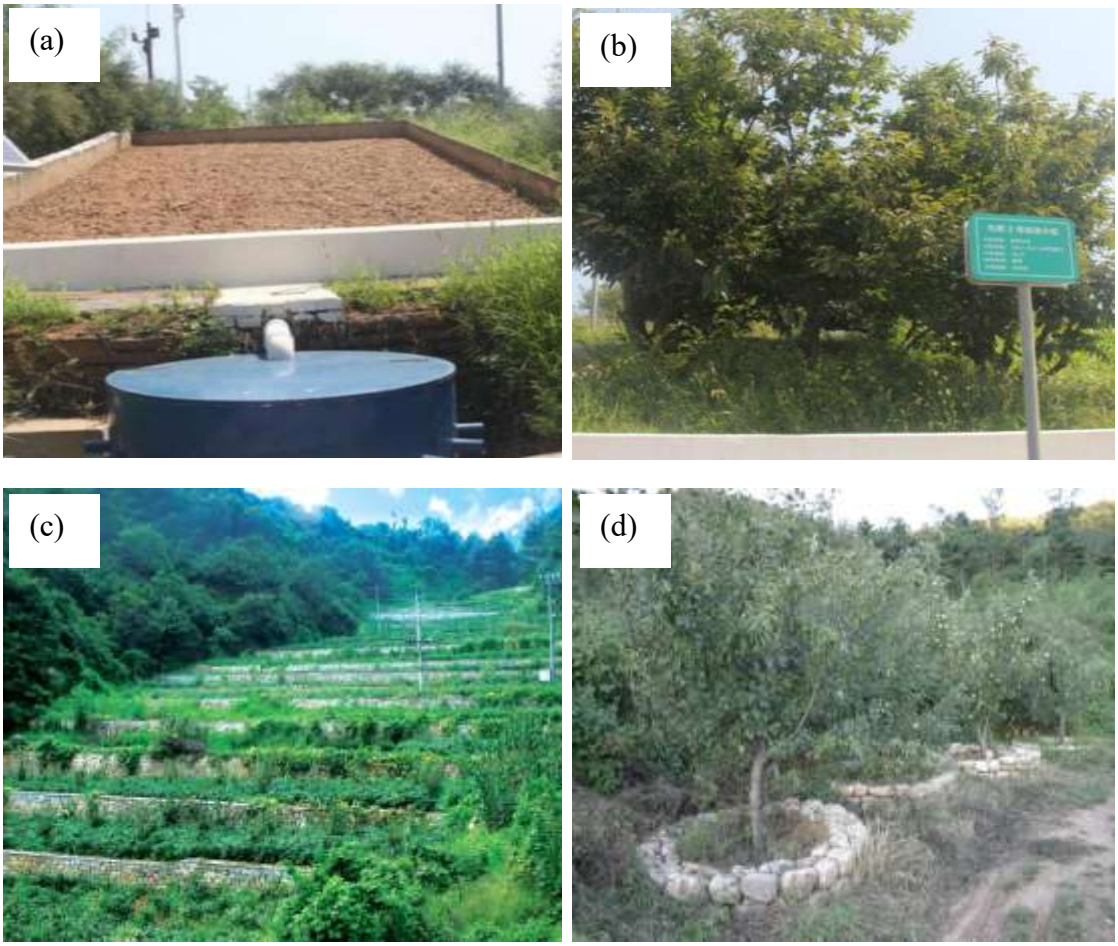

714 **Fig. 3**

715

716

717

718

719

720

721

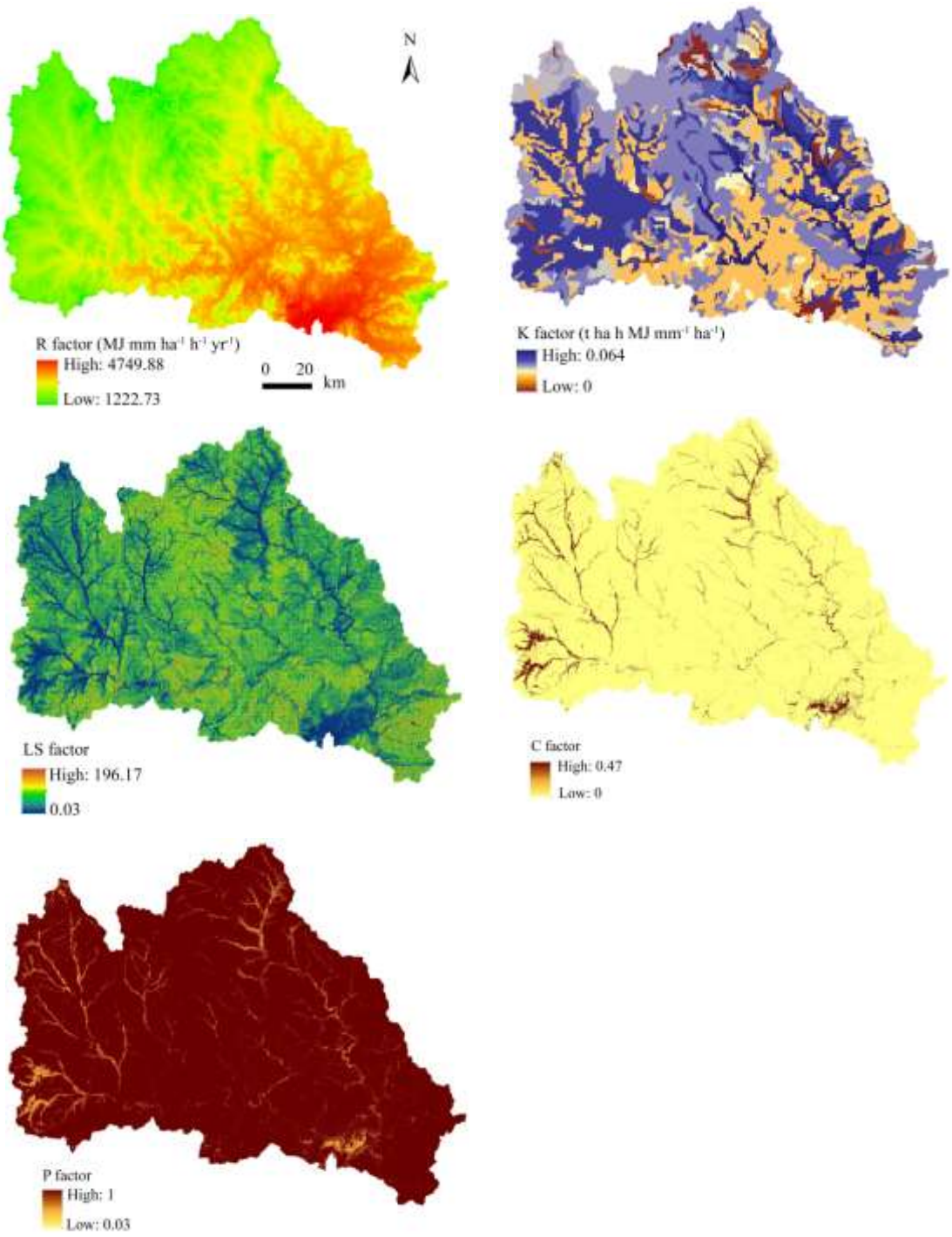
N
R factor (MJ mm ha⁻¹ h⁻¹ yr⁻¹)
High: 4749.88
Low: 1222.73
0 20 km
K factor (t ha h MJ mm⁻¹ ha⁻¹)
High: 0.064
Low: 0
LS factor
High: 196.17
0.03
C factor
High: 0.47
Low: 0
P factor
High: 1
Low: 0.03

Fig. 4

728

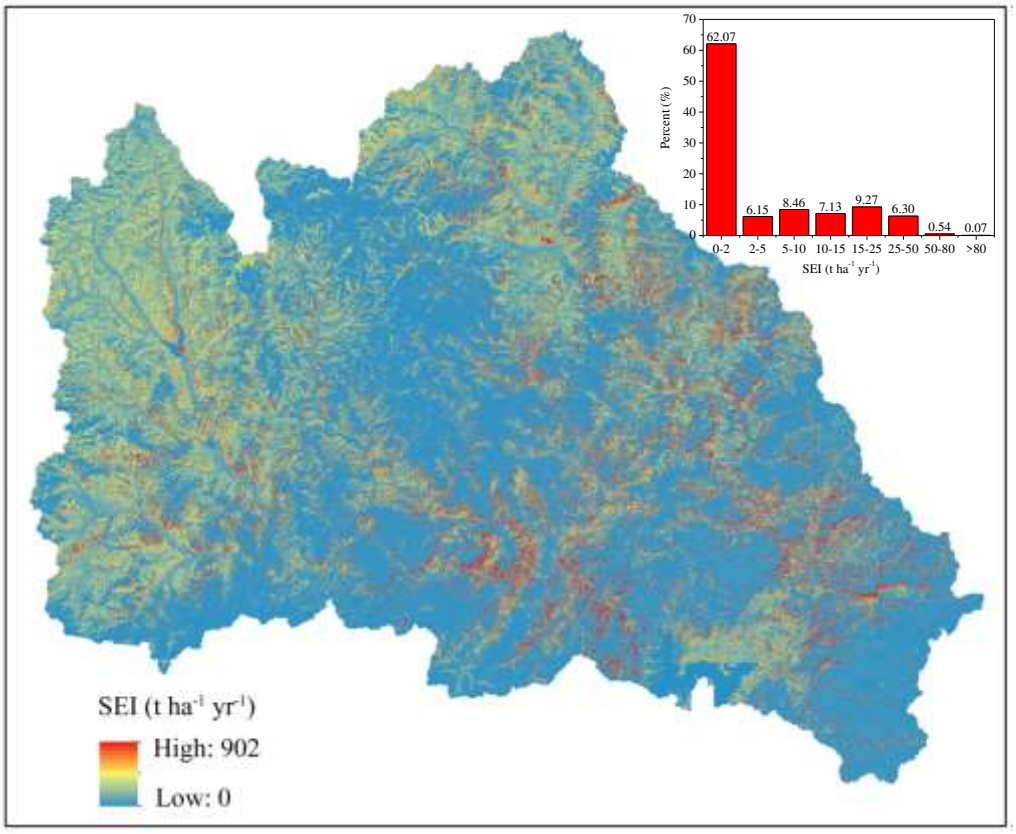

729 **Fig. 5**

730

731

732

733

734

735

736

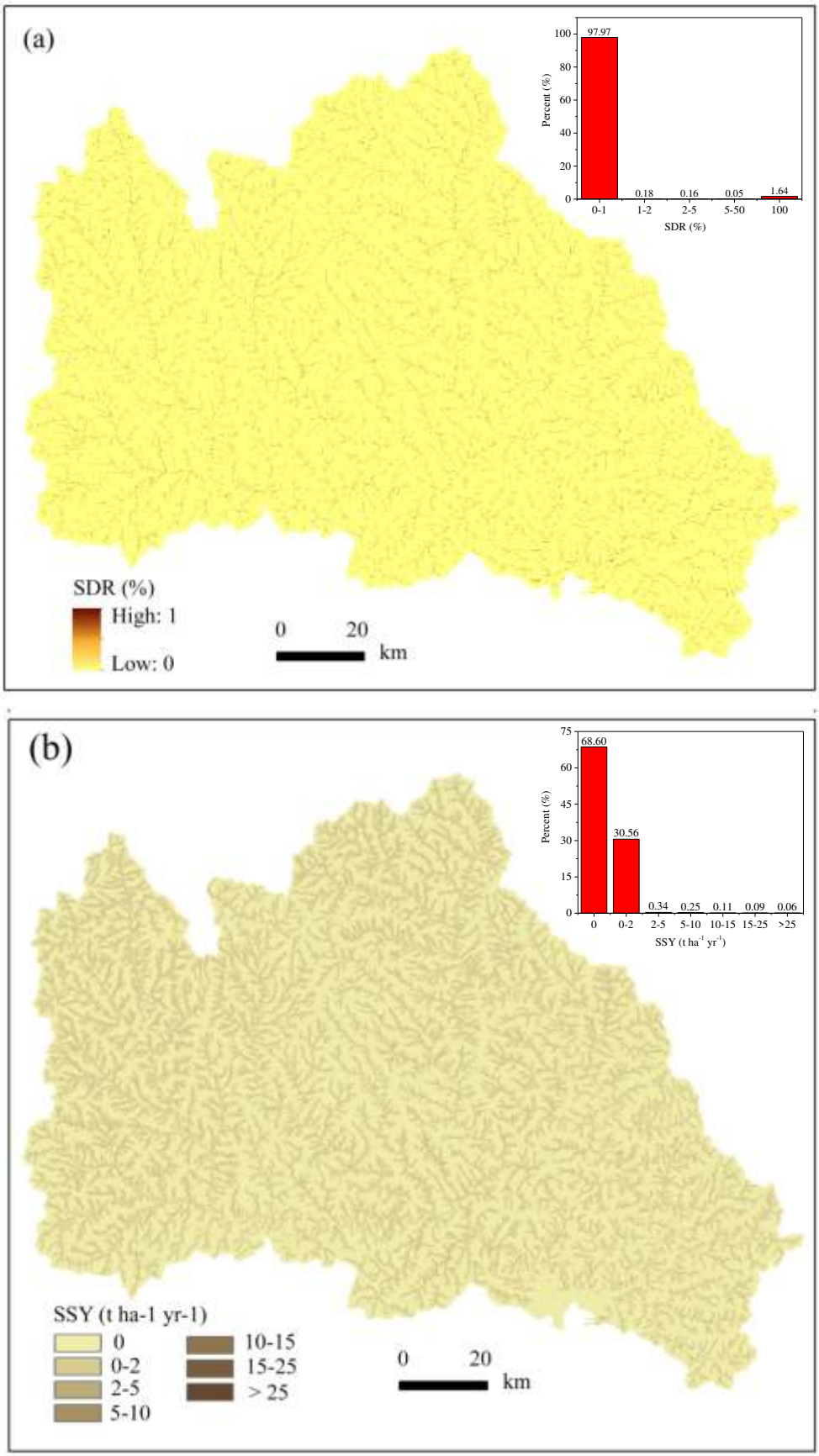
(a)
97.97
0.18
0.16
0.05
1.64
Percent (%)
0-1
1-2
2-5
5-50
100
SDR (%)
SDR (%)
High: 1
Low: 0
0
20
km
(b)
68.60
30.56
0.34
0.25
0.11
0.09
0.06
Percent (%)
0
0-2
2-5
5-10
10-15
15-25
>25
SSY (t ha-1 yr-1)
SSY (t ha-1 yr-1)
0
0-2
2-5
5-10
10-15
15-25
> 25
0
20
km

737

Fig. 6

738

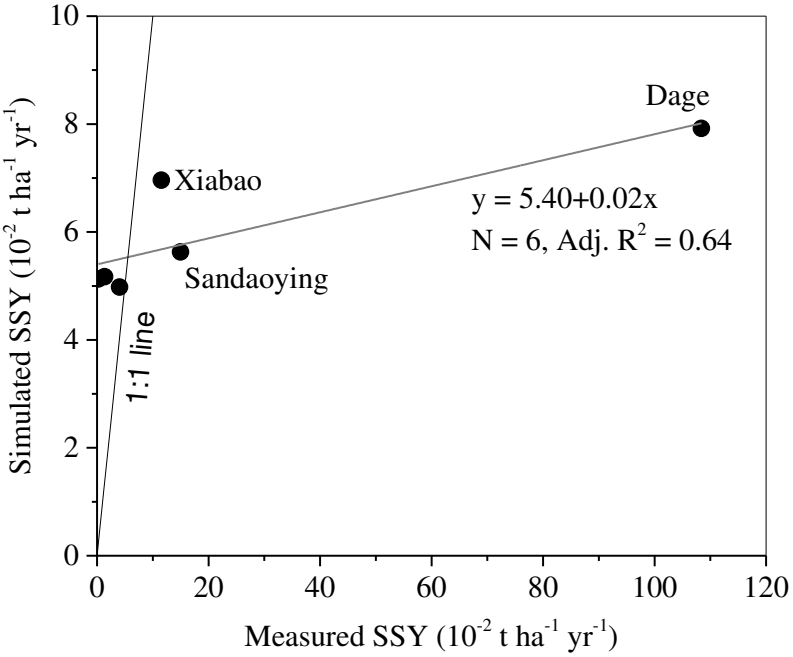

739 **Fig. 7**

740

741

742

743

744

745

746

747

748

749

750

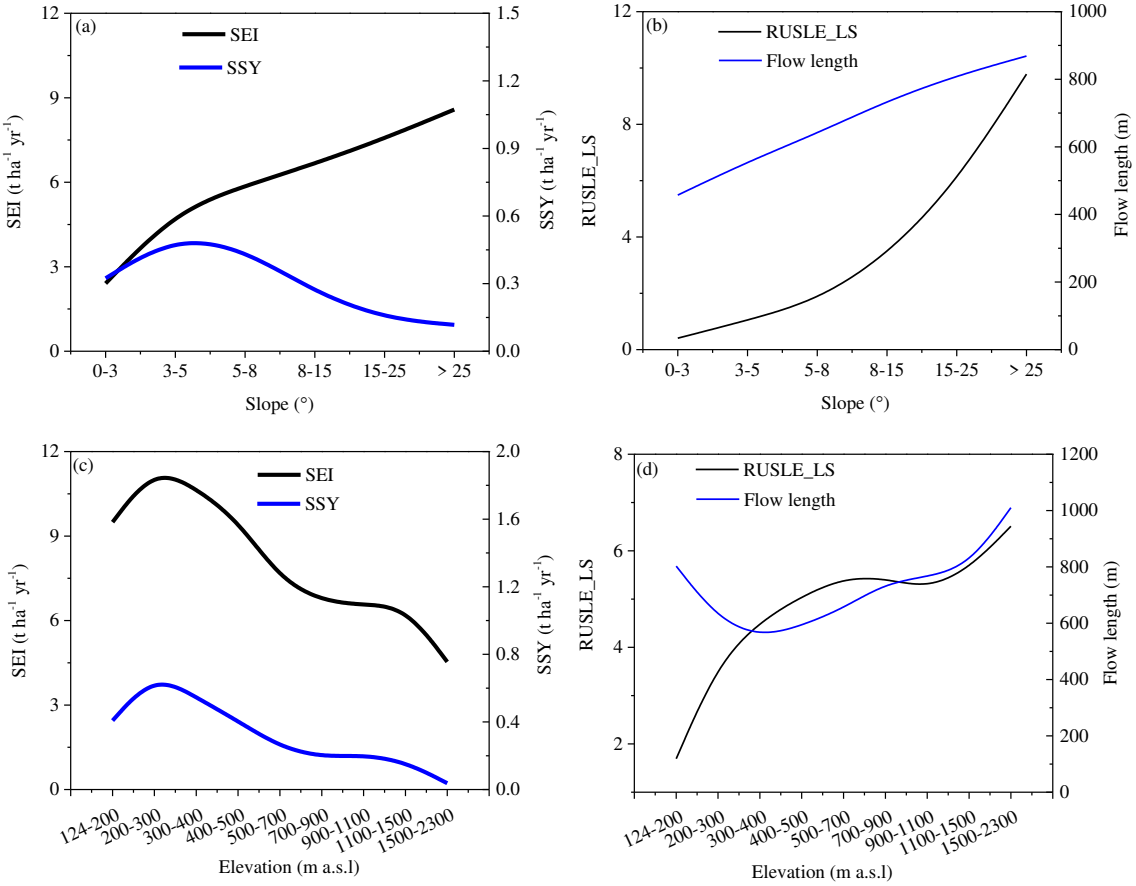
(a)
SEI
SSY
SEI (t ha-1 yr-1)
SSY (t ha-1 yr-1)
Slope (°)
0-3
3-5
5-8
8-15
15-25
> 25
(b)
RUSLE_LS
Flow length
RUSLE_LS
Flow length (m)
Slope (°)
(c)
SEI
SSY
SEI (t ha-1 yr-1)
SSY (t ha-1 yr-1)
Elevation (m a.s.l)
124-200
200-300
300-400
400-500
500-700
700-900
900-1100
1100-1500
1500-2300
(d)
RUSLE_LS
Flow length
RUSLE_LS
Flow length (m)
Elevation (m a.s.l)

Fig. 8

Figures

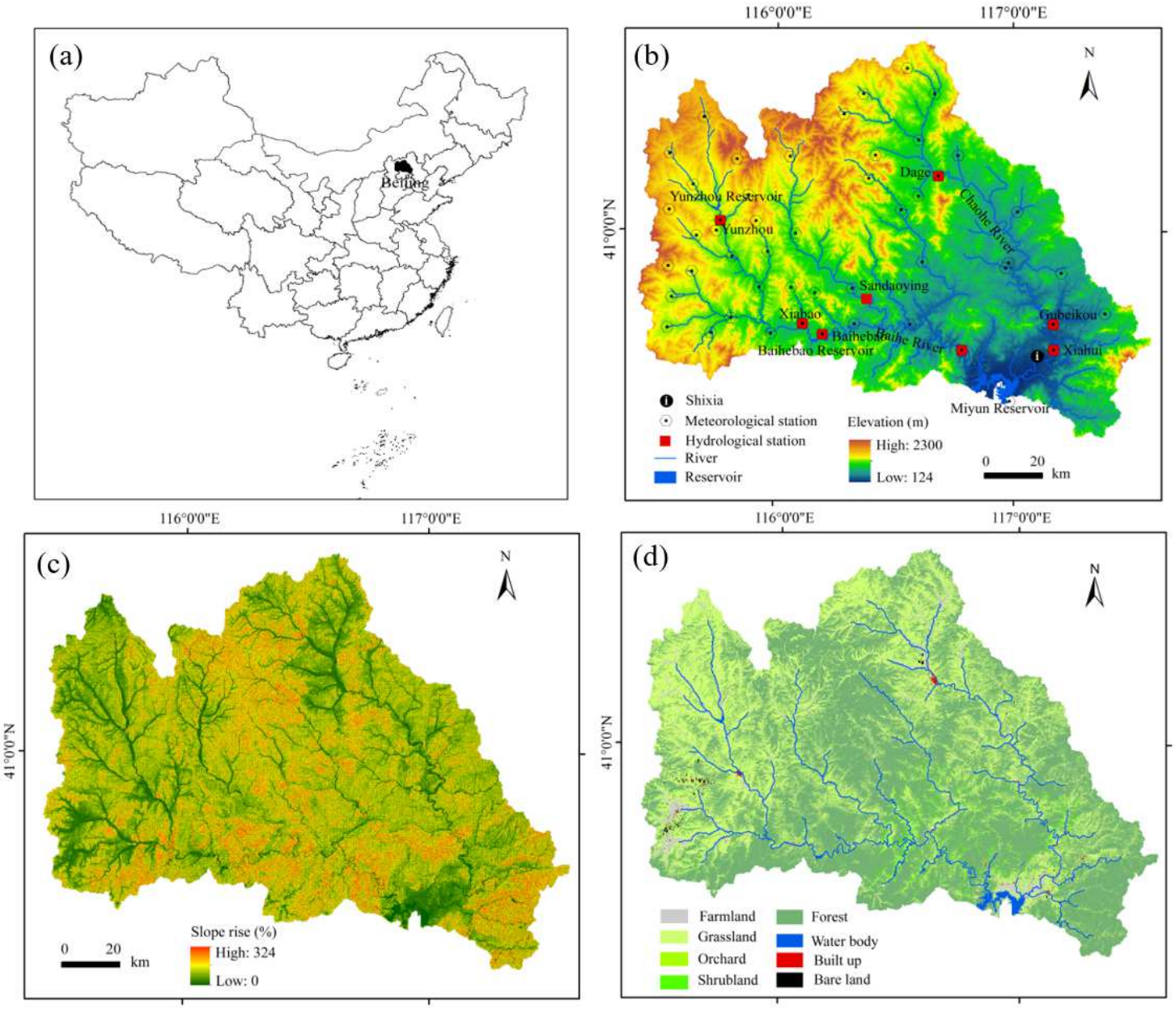

Figure 1

Maps showing (a) location of the catchment upstream of the Miyun Reservoir, (b) the distributions of hydrological stations, meteorological stations, Shixia subcatchment, reservoirs, and the elevation range, (c) slope gradient, and (d) land use types Note: The designations employed and the presentation of the material on this map do not imply the expression of any opinion whatsoever on the part of Research Square concerning the legal status of any country, territory, city or area or of its authorities, or concerning the delimitation of its frontiers or boundaries. This map has been provided by the authors.

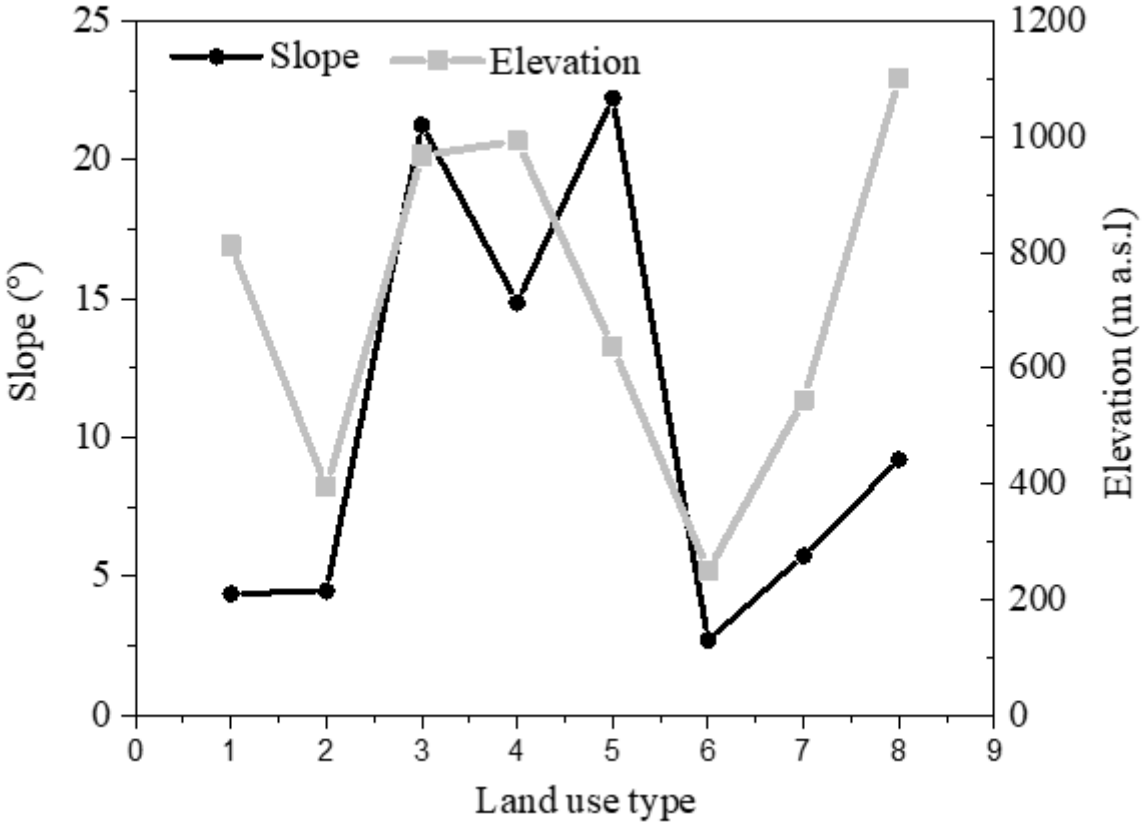

Figure 2

The mean slope gradients and elevations of different land use types distributed in the study catchment. Note:the numbers in the x-axis represent land use types in Table 7

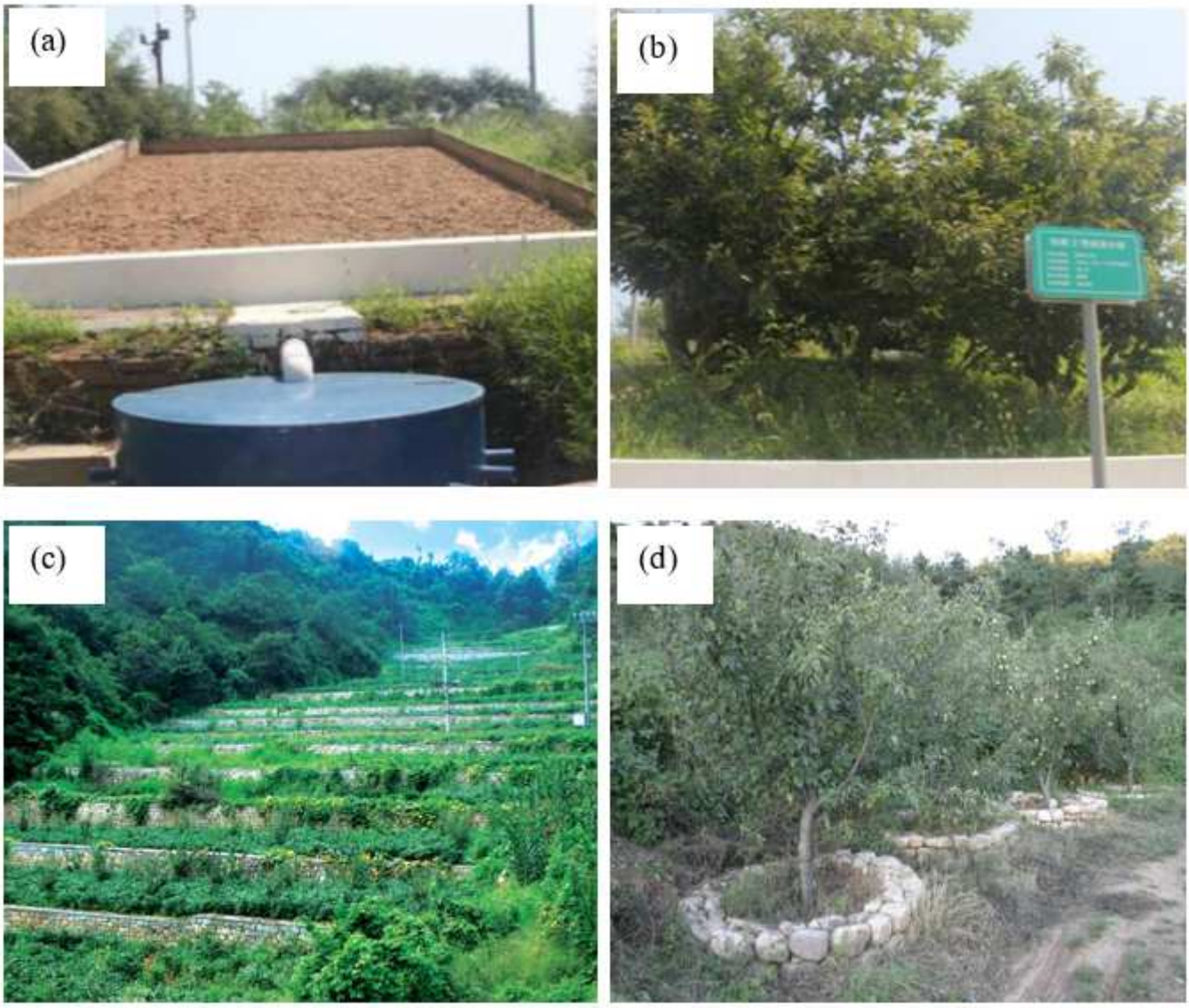

Figure 3

Pictures showing (a) runoff plot with bare soil, (b) forest, (c) terraced farmland, and (d) tree tray in the orchard field

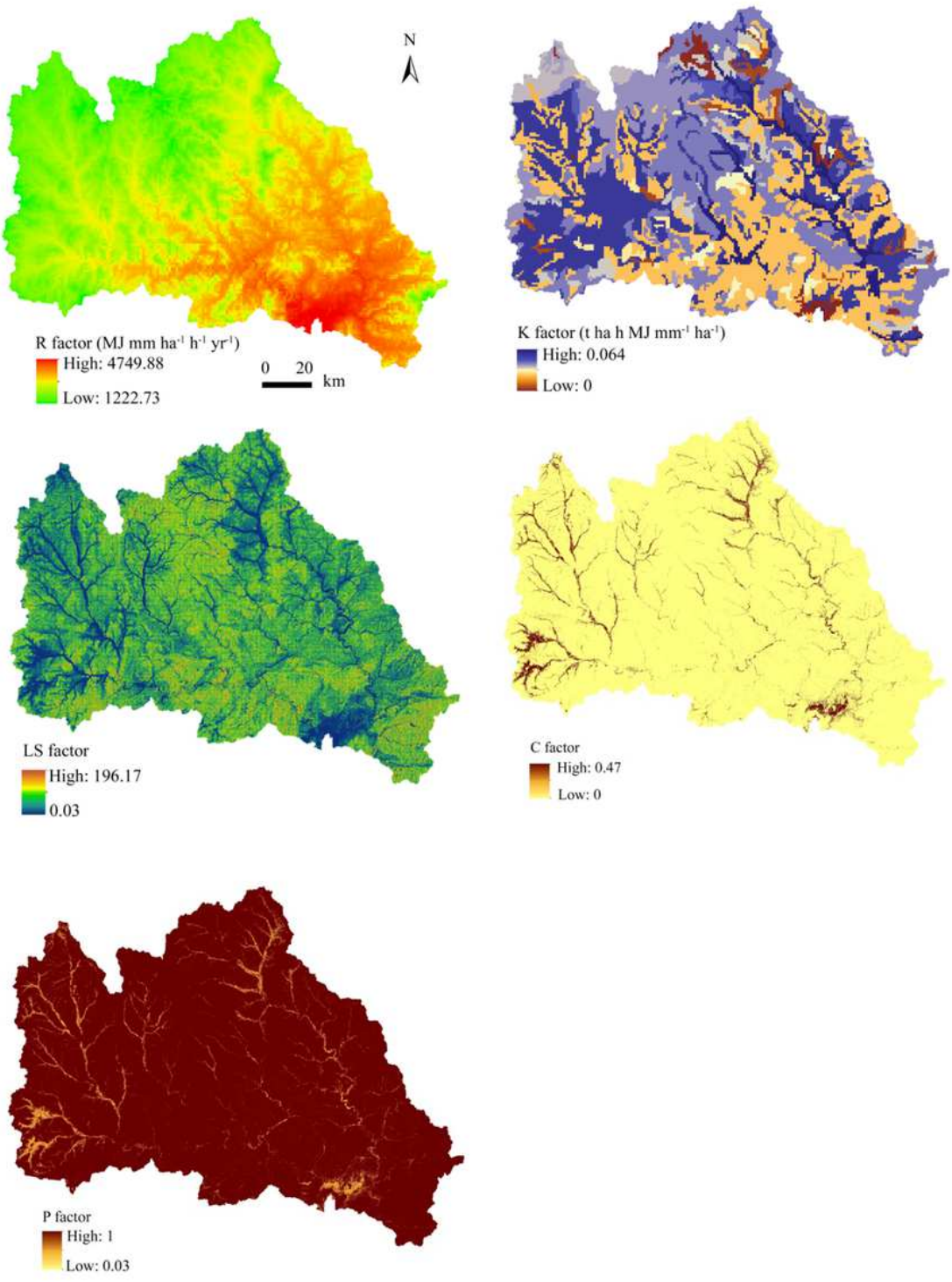

Figure 4

Spatial distributions of the values of RUSLE-R, -K, -LS, -C, and -P factors in the study catchment Note: The designations employed and the presentation of the material on this map do not imply the expression of any opinion whatsoever on the part of Research Square concerning the legal status of any country, territory, city or area or of its authorities, or concerning the delimitation of its frontiers or boundaries. This map has been provided by the authors.

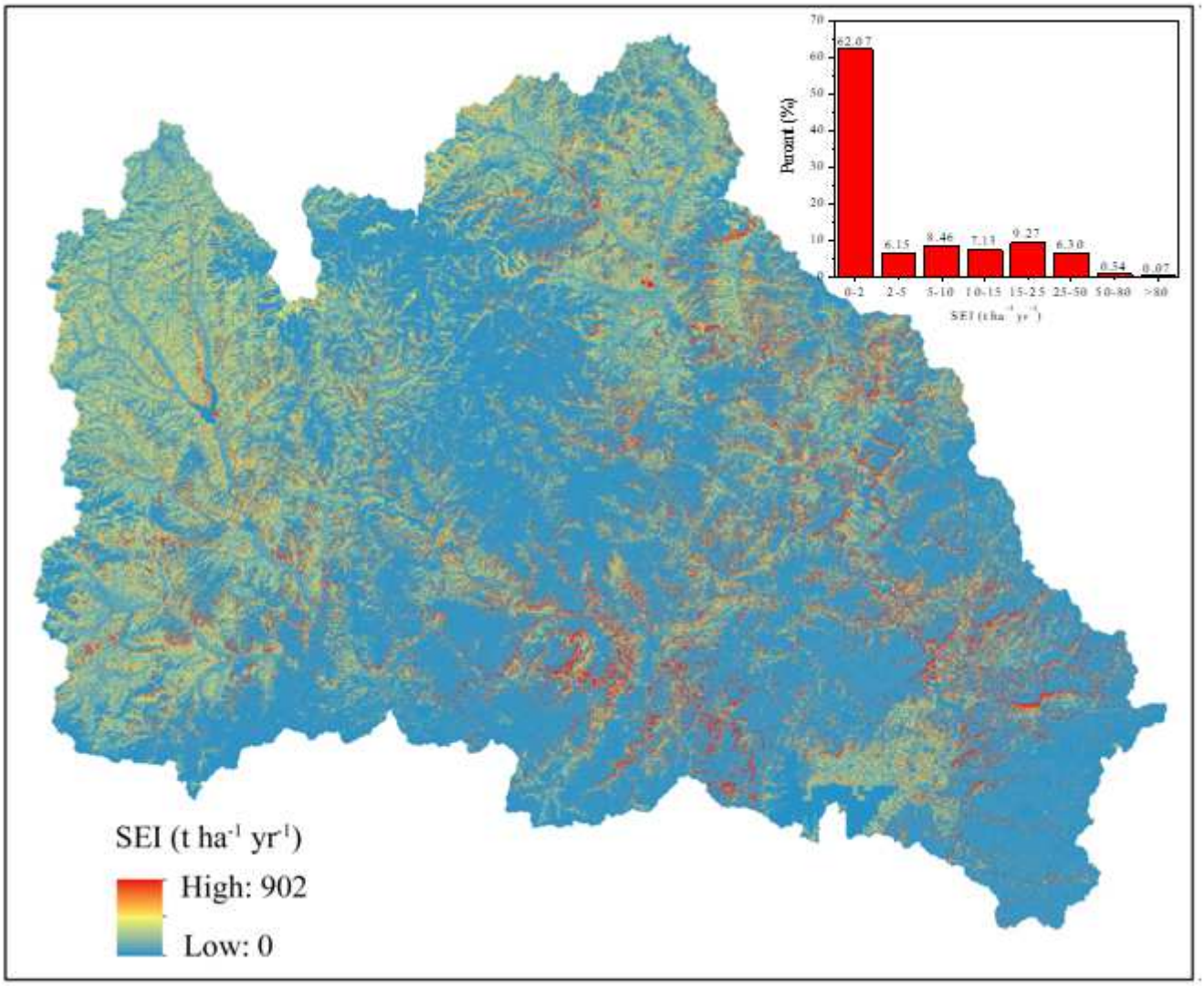

Figure 5

Spatial distribution of the estimated soil erosion intensity (SEI) in the study catchment Note: The designations employed and the presentation of the material on this map do not imply the expression of any opinion whatsoever on the part of Research Square concerning the legal status of any country, territory, city or area or of its authorities, or concerning the delimitation of its frontiers or boundaries. This map has been provided by the authors.

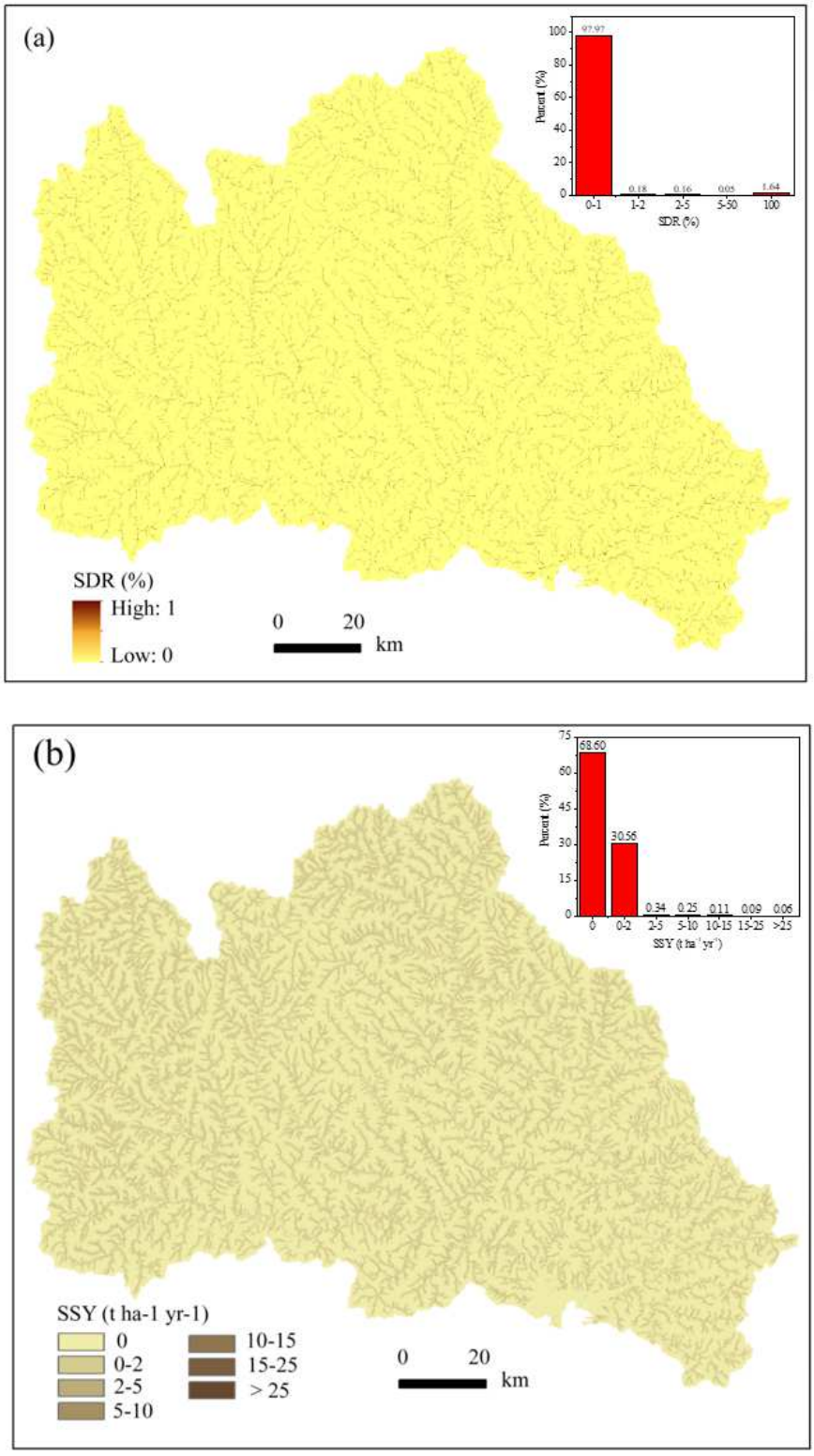

Figure 6

Map showing the spatial distributions of the estimated SDR (a) and SSY (b). Note: The designations employed and the presentation of the material on this map do not imply the expression of any opinion whatsoever on the part of Research Square concerning the legal status of any country, territory, city or area or of its authorities, or concerning the delimitation of its frontiers or boundaries. This map has been provided by the authors.

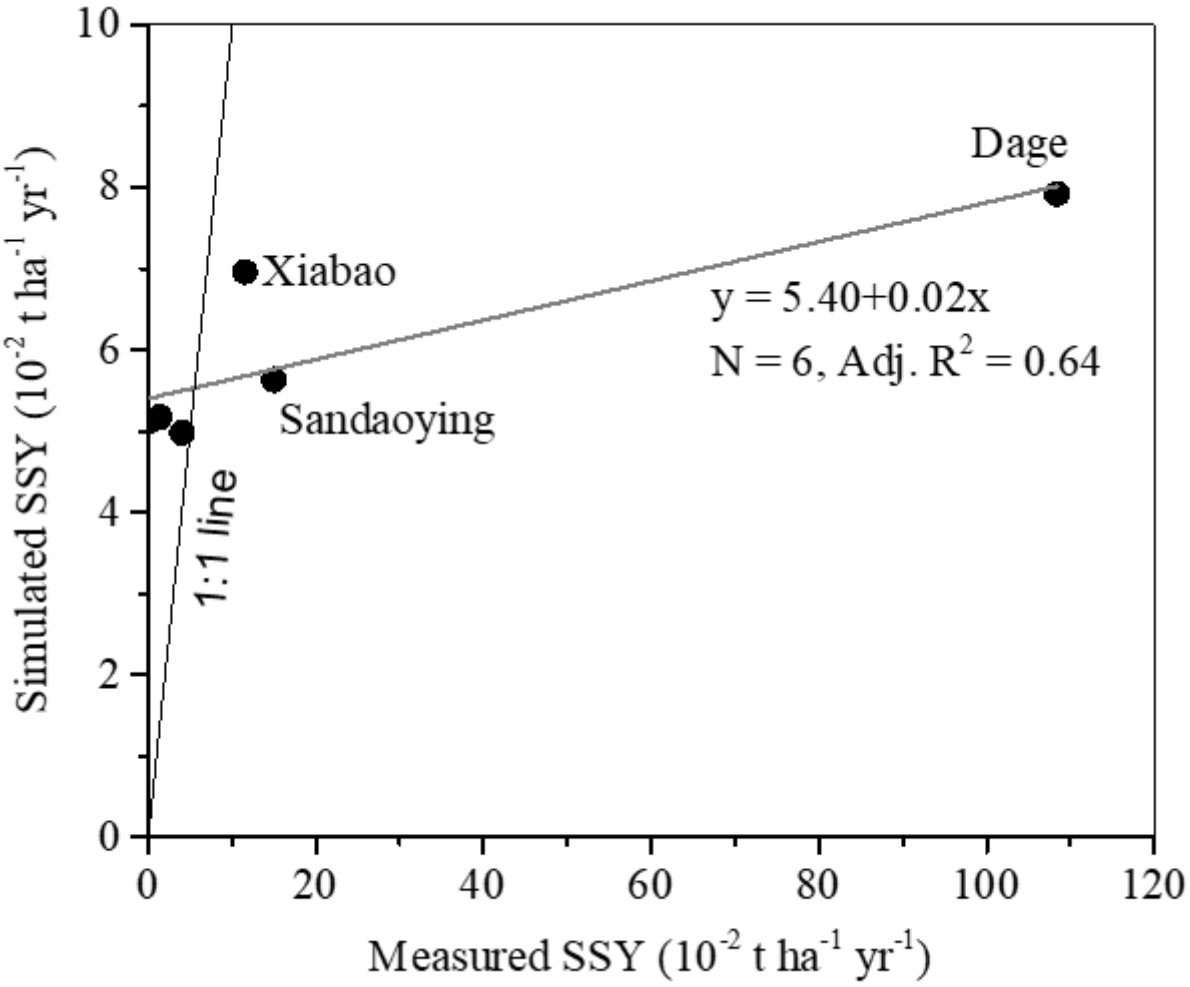

Figure 7

Comparison between the measured SSY with the simulated ones for the six subcatchments in Table 1

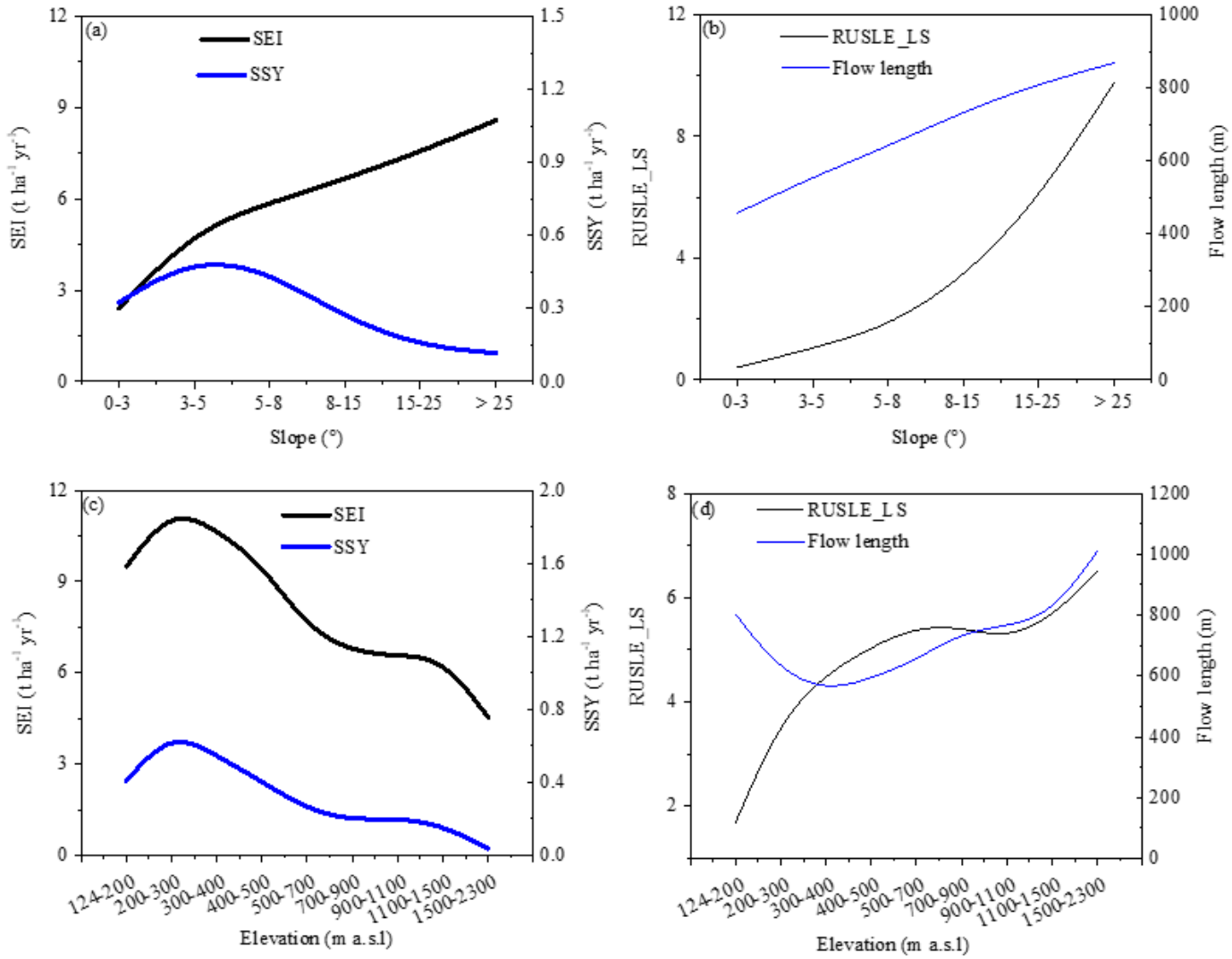

Figure 8

Soil erosion intensity (SEI) and SSY (ac), and RUSLE-LS factor and flow length of the cells to the nearest channels with increasing slope gradients and elevations (bd)